2 Electrochemical and Optical Oxygen Microsensors for *In Situ* Measurements

R. N. GLUD
University of Copenhagen, Denmark
J. K. GUNDERSEN AND N. B. RAMSING
University of Aarhus, Denmark

In Situ Monitoring of Aquatic Systems: Chemical Analysis and Speciation Edited by J. Buffle and G. Horvai.

1 INTRODUCTION

1.1 TECHNIQUES FOR MEASURING DISSOLVED O_2

1.1.1 Laboratory Techniques

Oxygen (O_2) is an absolutely critical key molecule in nature. Oxygen is produced by photosynthesis, and it is the ultimate electron acceptor for degradation of organic material. It is thus an excellent tracer for biological activity in the pelagic environment. Adequate availability of molecular oxygen is a prerequisite for most fauna and flora, and microbial processes are largely governed by the availability of oxygen as a terminal electron acceptor. In an evolutionary perspective, the advent of oxygenic photosynthesis and the gradual oxidation of the biosphere was thought to be essential to the subsequent evolution of multicellular organisms and all higher life forms. Because of its universal importance numerous techniques for measuring dissolved O_2 have been developed and have been applied with variable success to the aquatic environment.

The iodometric titration technique [1] probably represents the oldest and most widely applied method for O_2 determination and it is still used with only minor modifications since the original description. Techniques such as gasometry [2], mass spectrometry [3] and gas chromatography [4] have been employed, but have never become widely used, and they were not well suited for *in situ* applications. Various polarographic and voltammetric measuring principles have been applied for O_2 sensing especially within the fields of medicine and physiology [5–11]. Voltammetric O_2 measurements will be discussed in Chapter 9. However, amperometric O_2 sensors have probably been the most successful within the aquatic sciences and most certainly the most widely applied principle for *in situ* studies. The working principle of these sensors is based on the measurement of a current that is proportional to the rate at which O_2 is reduced on a metal surface kept at a fixed negative potential (around -0.8 V). Numerous amperometric macrosensor designs for pelagic work and *in*

situ respirometry have been presented in recent decades and the field has been extensively reviewed [12–15]. The aim of this review is thus not to provide a comprehensive overview of all O_2 sensors applied in aquatic science. Rather we would like to present insights into the possibilities of performing O_2 analysis using O_2 microsensors, with emphasis on *in situ* measurements, that have evolved since Revsbech and Jorgensen [16] reviewed the use of microelectrodes in microbial ecology.

Basically two types of O_2 microelectrodes have been applied *in situ*; cathode- and Clark-type sensors. Recently, microsensors based on optochemical measuring principles have successfully been introduced to aquatic science and have demonstrated great potential for *in situ* applications in the water column as well as for benthic studies.

1.1.2 Water Column and Sediment–Water Interface Studies

Most *in situ* work has been performed in the pelagic environment. Here constraints on sensor size, power supply, data transmission etc. are less than for studies across the sediment–water interface. This is simply because in the water column the spatial and temporal scales for O_2 variability are several orders of magnitudes larger than the variability found across the sediment–water interface. In this chapter we apply the term interface for the boundary between sediment and water. The vertical O_2 gradient in the water column typically extends over depth scales of meters (or hundreds of meters) and O_2 concentrations may be stable for hours or days [17]. The size of sensors and associated electronics is therefore of minor importance and often constant cable connections between ship and equipment put few constraints on the power requirements.

At the interface O_2 gradients are very steep and the characteristic depth scales are on the order of mm or μm [18]. Additionally, the O_2 concentration across such interfaces may change drastically within seconds as a result of changes in hydrodynamics, the faunal activity, or photosynthesis. Meaningful measurements at interfaces therefore put severe constraints on the applied sensors in terms of size, response time and stirring sensitivity. Operation at such a small scale also makes a constant cable connection to a ship problematic since mechanical disturbance via the cable can affect the position of the sensors.

The introduction of microsensors to aquatic science in the early eighties opened many new research fields, especially for benthic research [19–21]. Additionally, the miniaturization offered several advantages over the more commonly applied macro-(or mini-) sensors (see below), although these advantages have not yet been widely appreciated and exploited. Oxygen microsensors are therefore only gradually being introduced to studies in the water column and for *in situ* respirometry [22,23].

Various definitions for a microsensor have been used (see Chapter 1). In the following we have chosen to use a rather broad definition stating that an O_2 microsensor is any sensor that is capable of measuring the O_2 distribution with a spatial resolution better than 100 μm.

1.2 O_2 MICROSENSORS

The main advantage of microsensors is the very small size of the sensing tip. This allows measurements at the same scale as the structures relevant for production or consumption of O_2 in the aquatic environment [16,24–28]. However, the miniaturization also makes it possible to exploit working principles that would not work at macroscale. This is because on a small scale diffusion is a very efficient transport mechanism and thus scaling down improves signal stability, and reduces the response time and the analyte consumption rates.

The first O_2 microsensors were simple bare platinum cathodes. However, in order to provide a chemical and physical shielding towards the environment most cathode sensors that have been applied were coated with membranes [29–31] (Figure 1A). The membrane must allow O_2 to penetrate, but at the same time it must be electrically conducting. This means that at least some ions must be able to pass the membrane, this can cause interference problems with other solutes in the environment (see section 2.6). Various membrane materials have been utilized within different fields of research: Collodion, polystyrene, Zapon Lacquer, silicone, acrylic polymers, cellulose acetate, DPX resin etc. [32–34]. The different materials have their advantages and disadvantages in relation to adhesion, mechanical stability, permeability towards O_2 and various electrolytes, etc. The optimal membrane material for a given application has to be carefully evaluated. For applications in benthic research DPX-membranes have proven to be successful [33,35]. The polarogram of gold-plated cathodes has a broader plateau around −0.8 V than that of platinum cathodes [32]. This gives rise to a more stable current, which is less affected by small physical or biological fluctuations during application. Most microelectrodes therefore operate with a gold-plated cathode. The tip diameter of cathode-type sensors can be made very small (<1 μm) and they have proven very useful for physiological studies [32]. The very first field and *in situ* deep-sea measurements were performed with such sensors and they are still occasionally being applied *in situ* [35–37]. In order to increase the signal size and the robustness of such sensors the so-called needle-electrodes with tip diameters in the order of 600–800 μm have been developed and applied in situ [38,39]. Figure 1 schematically present the outlines of cathode-type sensors. A major improvement in O_2 microsensing was achieved by miniaturizing the Clark-type O_2 sensor [40,41]. As compared with the cathode-type sensor the Clark-type sensor is more complicated to manufacture, but has some major advantages (see below).

Some typical sensor characteristics for micro- and mini-sensors that have been applied for benthic *in situ* studies are compiled in Table 1. However, the sensor properties of individual electrodes vary, so the tabulated values can only

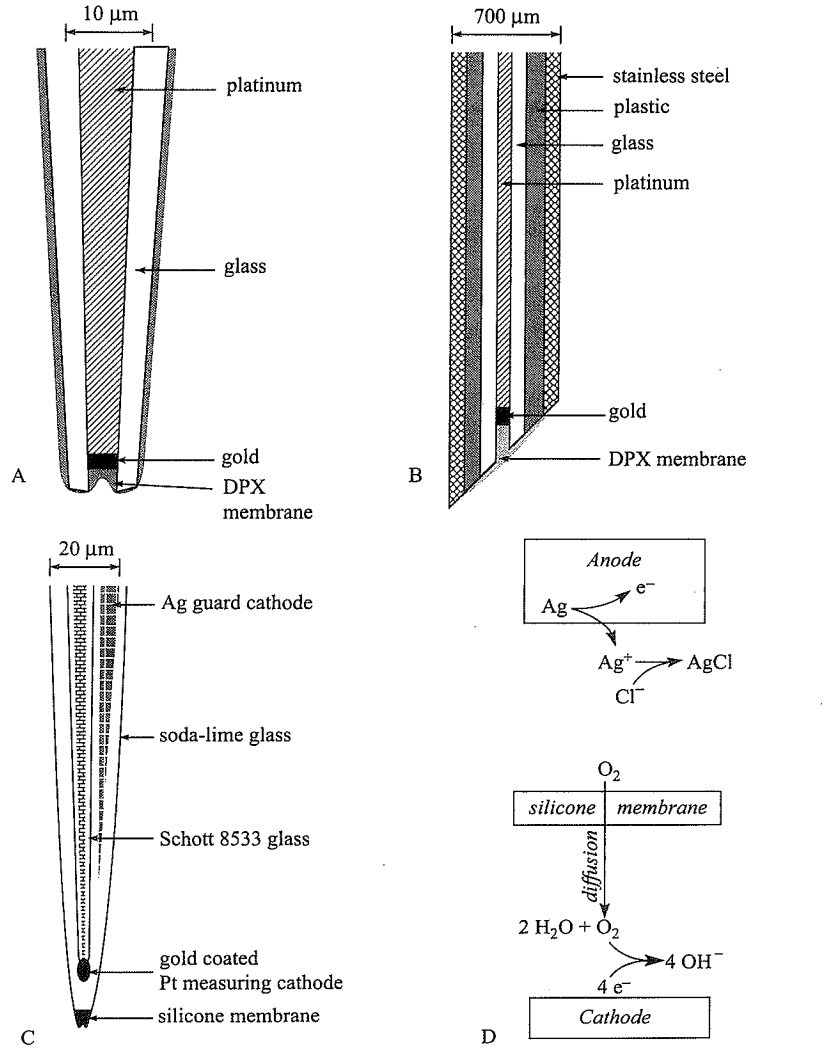

Figure 1. (A) The basic structure of a gold-plated and DPX-coated cathode sensor. (B) The tip zone of a needle-type DPX-coated cathode sensor. (C) The tip of a Clark-type O_2 microelectrode. The anode which is usually fixed further up in the casing is not shown. (D) Schematic drawing of the measurement principle. The upper panel shows the reaction at the anode placed in the bulk electrolyte, while the lower panel illustrates the reaction at the negatively polarized cathode (DPX: see glossary)

Table 1. Characteristics of three types of amperometric O_2 sensors applied for *in situ* interface studies

	Sensor		
	Micro-cathode*	Micro-Clark	Needle-type
Tip size (μm)	0.2–5	1–10	600–800
Stirring sensitivity (%)	2–50	0–2	5–50
90% Response time (s)	0.1–2	0.5–2	60–120
Detection limit ($\mu mol\,L^{-1}$)	0.1	0.1	1
Signal size at air saturation (pA)	100–200	50–200	5000
Main interference	Mg^{2+}, Ca^{2+}, H_2S	H_2S	Mg^{2+}, Ca^{2+}, H_2S
Key references	32–34	45	38, 39

* Membrane coated.

be taken as typical electrode performance. It should also be stressed that the importance of various sensor characteristics must be evaluated in the context of the scientific question addressed. In some instances, stirring sensitivity may be crucial for the interpretation of recorded data while it is irrelevant in others. The most appropriate sensor properties therefore vary with a given task. In the following section the various sensor characteristics are discussed in detail and examples of applications where sensor characteristics are of major importance are presented and discussed.

For water column studies instrument packages (so-called conductivity–temperature–depth instruments or CTDs) capable of carrying O_2 macrosensors have been commercially available for many years. Most available systems are modular and the configurations are custom designed, and optimized for a given application. For *in situ* microsensor studies at the benthic interface various *in situ* vehicles have been constructed and applied. Independently operating platforms working directly at the sea floor for interface studies are termed 'landers'. A review of technical solutions and designs of benthic landers was recently presented [42]. Further, instrumental concerns in relation to *in situ* measurements in the benthic boundary layer have also been discussed recently [43] and special attention to *in situ* measurements with microsensors was given by another recent review [44]. In the present context we will therefore refrain from further discussion on *in situ* instrumentation and will refer to the above-mentioned reviews.

2 CLARK-TYPE O_2 MICROELECTRODE

2.1 CONSTRUCTION AND FUNCTION

The measuring cathode of the Clark-type O_2 microsensor is immersed in an aqueous electrolyte chamber which contains the internal Ag/AgCl reference

anode (Figure 1C). The alkaline electrolyte (pH 10) of a standard microelectrode contains $0.5\,mol\,L^{-1}$ KCl in $0.5\,mol\,L^{-1}$ carbonate buffer. The internal solution and electrodes are separated from the exterior by a glass casing and an O_2 permeable silicone membrane (Figure 1C). A silver anode within the electrolyte acts as the reference anode. An additional improvement of the sensor was made by placing a guard cathode behind the sensing cathode [45] (Figure 1C). This prevented interference from O_2 diffusing toward the sensor tip from the bulk electrolyte chamber within the electrode and thereby ensured a constant low zero-current. A review of the construction of the Clark-type O_2 microsensor can be found elsewhere [16].

In the working mode the measuring and the guard cathode are both polarized at $-0.8\,V$ versus the Ag/AgCl reference electrode. Lower polarization may result in an inefficient reduction of O_2 (low unstable signals), while higher polarization may lead to reduction of water (high unstable signals) followed by gas formation and insensitivity. The measuring cathode consists of a gold-plated platinum wire. The reaction stoichiometry at the cathode is shown in Figure 1D. The redox reaction of O_2 is very complex and not completely understood, but H_2O_2 is known to be an important intermediate [46]. A porous structure of the gold surface making up the measuring cathode gives a very large catalytic area, ensuring a complete reduction of oxygen and thus a stable signal. During measurements, there is a net diffusion of O_2 through the highly permeable silicone membrane. The oxygen is dissolved in the electrolyte and is subsequently reduced at the gold-coated platinum cathode. The Clark-type O_2 microsensor thus responds to the O_2 partial pressure of the medium which is determined by the O_2 concentration and other environmental parameters such as temperature, salinity etc. (see below). At the reference anode solid Ag is oxidized and subsequently precipitates as AgCl (Figure 1D).

2.2 CALIBRATION (TEMPERATURE AND SALINITY EFFECTS)

In the case of constant temperature, salinity and pressure, the Clark-type microsensor has a perfectly linear response to O_2. In most *in situ* applications it is a simple matter to perform a two-point calibration by measuring the electrode signal in two different water samples whose O_2 concentration is subsequently determined by Winkler titration. Alternatively, for benthic microprofile measurements two calibration points are typically inherent in the measurements: the constant reading in the bottom water and a zero reading in the deep anoxic sediment [44]. All that is required is thus a Winkler determination of the oxygen concentration in the bottom water.

Often O_2 measurements at variable salinity and/or temperature are required [22,47]. Electrode calibration in such complex cases demands a quantitative understanding of signal dependence on sensor dimension, salinity and temperature. A multivariate analysis of electrode signals as a function of various

external variables has been applied in order to construct a calibration model for Clark-type sensors [48]. Even though such an empirical approach may be useful in special cases, it is not generally applicable as it is not based on a full understanding of the function of the sensor. A mathematical description of the essential transport processes within a Clark-type O_2 microsensor was recently developed [49]. The model assumes that the internal geometry of the tip zone is conical and that the sensor tip can be described by three radii, the length of the

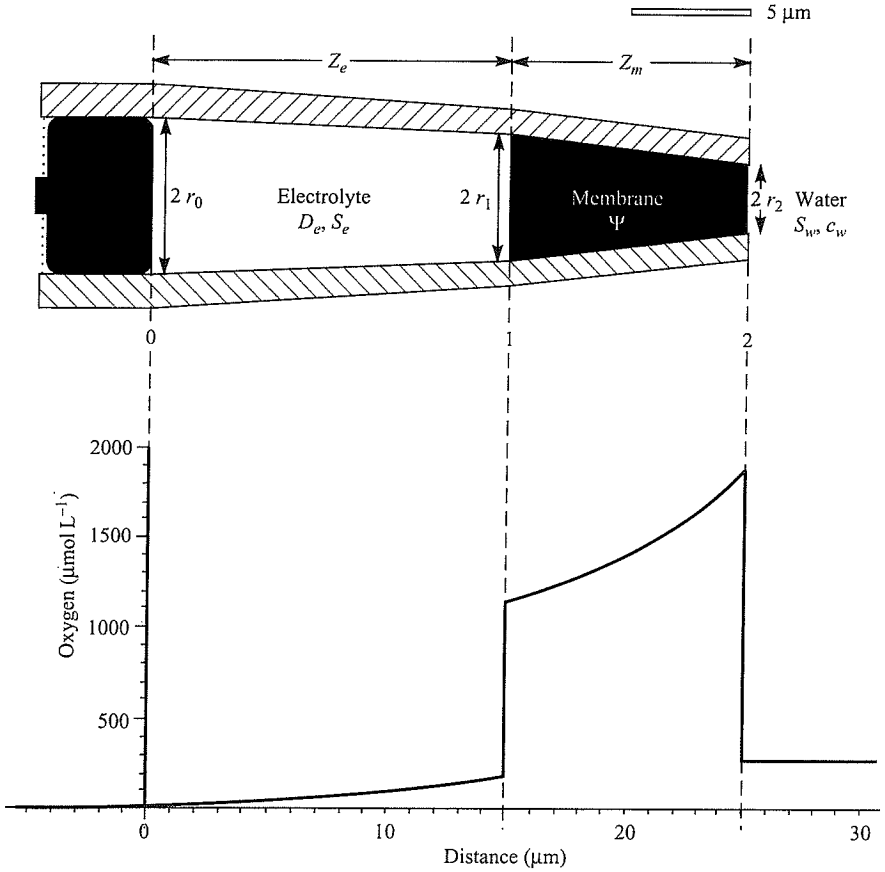

Figure 2. The tip of a Clark-type O_2 microelectrode as described by Equation (1). In case of the following physical conditions: $c_W = 273\,\mu mol\,L^{-1}$, $T = 295\,K$, salinity = 34‰, $Z_e = 15.0\,\mu m$, $Z_m = 10.0\,\mu m$, $r_0 = 3.4\,\mu m$, $r_1 = 2.8\,\mu m$, $r_2 = 1.5\,\mu m$, the sensor signal can be calculated from Equation (1) to be 259 pA. The resulting O_2 concentration profile through the tip zone is indicated. (Redrawn from Gundersen, J. K. *et al.*, *Limnol. Oceanogr.*, **43**, 1932 (1998). Reproduced by permission of American Society of Limnology & Oceanography.)

silicone membrane, and the distance between membrane and cathode surface (Figure 2). Additionally, two other assumptions are made: (i) the O_2 concentration at the cathode surface is zero (as is the case after a short polarization period) and (ii) the O_2 concentration at the outer silicone membrane surface equals the concentration in the bulk water phase. The latter assumption is only valid for sensors with low stirring sensitivity, yet the model can be extended to include the diffusive processes outside the sensor tip (this extension is discussed in section 2.3). In such a case the electrode signal, Si, given by the O_2 reduction current (i.e. sensor output minus zero current) can be described by applying simple Fickian diffusion theory and mass conservation [49,50]:

$$Si = \Phi\pi r_1 p_w \left(\frac{Z_m}{r_2\Psi} + \frac{Z_e}{r_0 D_e S_e}\right)^{-1} \quad (1)$$

where (for an explanation of symbols please also refer to Figure 2), Φ = current generated per mole O_2 reduced ($3.86 \times 10^{-5}\,A\,s\,mol^{-1}$), p_w = partial O_2 pressure in the ambient water (Pa), Z_m and Z_e = lengths of silicone membrane and electrolyte distance, respectively (m), Ψ = O_2 permeability of the silicone membrane (mol $m^{-1}\,Pa^{-1}\,s^{-1}$), D_e = O_2 diffusion coefficient in the electrolyte ($m^2\,s^{-1}$), S_e, S_w = O_2 solubility in the electrolyte or in water sample ($mol\,L^{-1}\,Pa^{-1}$), and r_0, r_1, r_2 = the internal sensor radii at the cathode, inner and outer position of the silicone membrane, respectively (m).

The geometry of a given sensor (r_0, r_1, r_2, Z_m and Z_e) can be determined with a microscope. The solubility, S_e, and the diffusion coefficients, D_e, can be found in the literature [51,52] and can be recalculated to the correct temperature and salinity [53]. The O_2 permeability, Ψ, (defined as the product of the diffusion coefficient of O_2 in the membrane material and the distribution coefficient between membrane and solution) of the silicone used for the sensor membranes has been measured to be $11.2 \times 10^{-15}\,mol\,s^{-1}\,m^{-1}\,Pa^{-1}$ [49]. However, the permeability of an electrode membrane at a given temperature is dependent on the degree of hydration and the age of the membrane. For most practical applications, it may be simpler to perform a one-point calibration for the determination of Ψ by applying equation (1). The model was experimentally verified by comparing the signal from 23 different O_2 microsensors to signals predicted by equation (1) (Figure 3). For this figure we used a fixed silicone permeability of $11.2 \times 10^{-15}\,mol\,s^{-1}\,m^{-1}\,Pa^{-1}$. The presented equation differs from previous calibration equations [54] in two ways: (i) it is a theoretical description of the molecular diffusion processes within the electrode, which does not rely on empirically determined relationships and (ii) it predicts the O_2 consumption of a given electrode.

If the value Z_e is 0 (i.e. the silicone membrane is coated directly on the cathode, as on a cathode microsensor), the signal becomes directly proportional

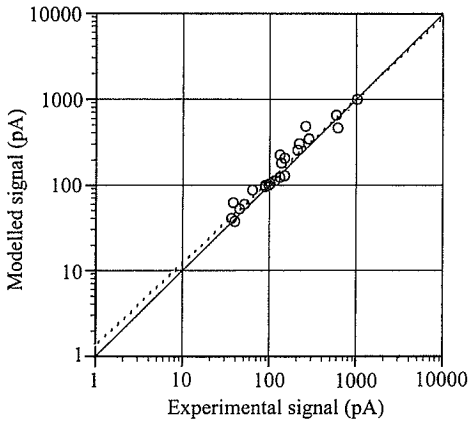

Figure 3. The signals of 23 Clark-type O_2 microelectrodes as calculated using equation (1) versus experimentally determined values. The solid line is the theoretical line with slope = 1 and ordinate at origin = 0, while the dashed line is the best linear fit. (From Gundersen, J. K. *et al.*, *Limnol. Oceanogr.* **43**, 1932 (1998). Reproduced by permission of American Society of Limnology & Oceanography.)

to the O_2 partial pressure multiplied by the membrane permeability and divided by the membrane length. This is in accordance with previous calibration equations for oxygen macro electrodes [54]. In Clark-type O_2 microsensors the distance Z_e typically accounts for 30–90 % of the internal diffusion distance and thus has to be included in a model of the electrode signal [49,55]. This can be demonstrated by model predictions of the sensor signal as a function of temperature and salinity. In the case of a constant O_2 concentration but an increased salinity of the bulk water surrounding the sensor, the partial pressure (p) will increase correspondingly. As the partial pressure is the only parameter in equation (1) affected by salinity, the sensor signal will increase irrespective of the membrane thickness (Figure 4A). The relative membrane thickness is defined as $(Z_m/Z_e) + Z_m$. If we instead increase the temperature, then the partial pressure (p), the permeability (Ψ), and the transport coefficient (D_e) will increase while the O_2 solubility (S_e) in the electrolyte will decrease; the combined effect will be a signal increase that will be more pronounced in case of thicker membranes (Figure 4B). Increasing the relative membrane thickness will result in relatively higher sensor signals and the effect will increase with temperature (Figure 4C) [49]. An earlier presented model described the sensor signal from a silver cathode, polyethylene-coated Clark-type macroelectrode [55]. The resulting equations bear resemblance to the model presented above.

The useful microelectrode signal is the sensor output minus the 'zero-current', i.e. the current at zero O_2 concentration. The zero-current is typically in the order of 1–2 pA (or approximately 1 % of the sensor signal in air-saturated

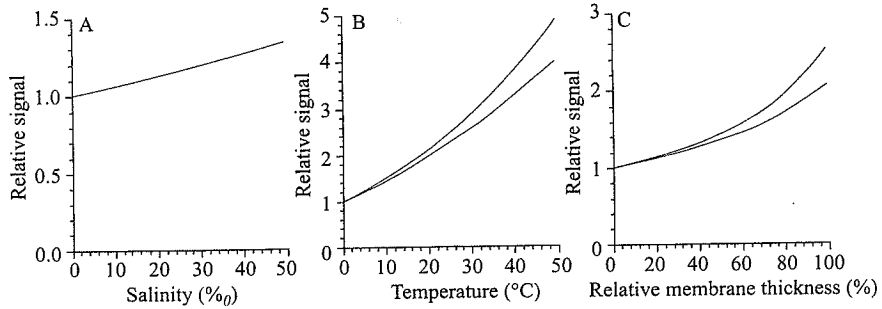

Figure 4. Relative signal change as a function of salinity (A) and temperature (B). The salinity effect is independent of the relative membrane thickness. However, the temperature-induced change is membrane thickness dependent as indicated by the upper (relative thickness 99.9 %) and the lower lines (relative thickness 0.1 %) in panel (B). Panel (C) presents the relative signal increase as a function of the relative membrane thickness at 50 °C (upper line) and 0 °C (lower line). (From Gundersen, J. K. *et al.*, *Limnol. Oceanogr.*, **43**, 1932 (1998). Reproduced by permission of American Society of Limnology & Oceanography.)

water). The zero-current is ascribed to conductivity and reducible constituents in the glass of the sensor [56], but minimal zero currents can be achieved by using highly insulating glasses. Measurements have shown that the size of the gold cathode has relatively little effect on the zero-current [56]. During long-term use of a microelectrode the zero-current typically decreases; this is partly due to a gradual consumption of O_2 dissolved in the electrolyte but may also be due to a gradual reduction of impurities in the glass. At high temperatures the zero-current may contribute significantly to the sensor signal (Figure 5) and it is therefore important to determine the zero-current at the working temperature. At elevated temperatures, for instance, it can be advantageous to reduce the polarization voltage in order to reduce the zero-current.

The model above contains only a single variable, the membrane permeability (Ψ), which has to be estimated at one known temperature and salinity (i.e. a one-point calibration). This one-point calibration allows for O_2 concentration determinations based on sensor signals obtained at any temperature and salinity. This makes calibration of microsensors for their application in water columns or in vent sites possible. The model also makes it possible to optimize sensor construction with respect to the signal to noise ratio, response time, and stirring sensitivity (see below).

2.2.1 Case Study: Measurements at a Vent Site

An extreme case of temperature effects on *in situ* measurements of O_2 is experienced during studies around hydrothermal vents, where temperatures

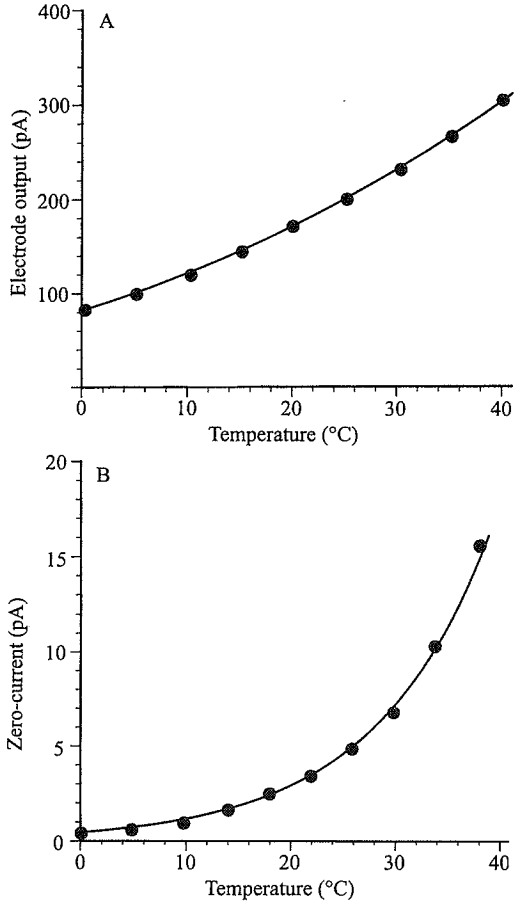

Figure 5. The output (A) and the zero current (B) as a function of temperature. (From Gundersen, J. K. *et al.*, *Limnol. Oceanogr.*, **43**, 1932 (1998). Reproduced by permission of American Society of Limnology & Oceanography.)

may vary from 1 to > 100 °C. In such cases a reliable calibration of the O_2 signals requires a good quantitative understanding of the temperature effects on the O_2 microsensor. During a study at 10 m water depth in the Aegean sea, O_2 and temperature microprofiles were recorded simultaneously at a variable distance from a vent center (Figure 6). It was observed that O_2 penetration depths and O_2 fluctuations at a given depth horizon gradually increased towards the vent center [57]. The simultaneously obtained temperature measurements expressed an extreme horizontal and vertical temperature gradient that had to be accounted for during sensor calibration (Figure 6).

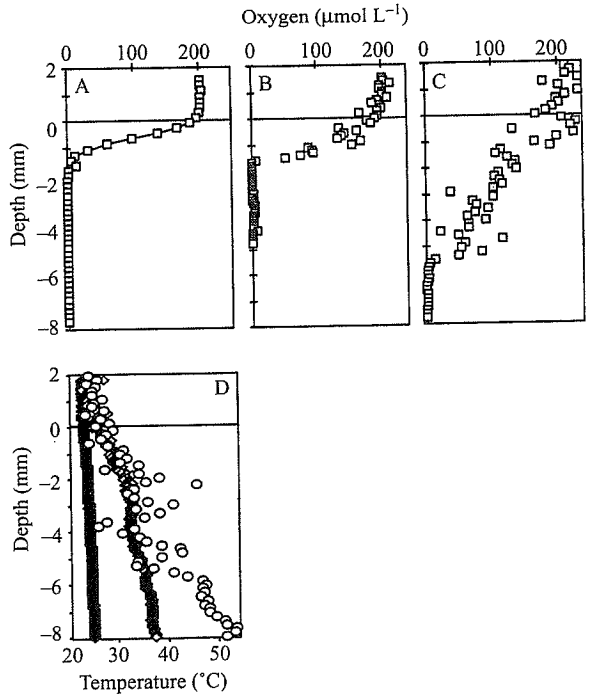

Figure 6. Panels (A), (B) and (C) show three microprofiles obtained *in situ* by Clark-type O_2 microelectrodes at distances of 4.0 m (A), 1.0 m (B) and 0.1 m (C) from a hydrothermal vent center. (D) illustrates the simultaneously obtained temperature microprofiles at the three respective sites (closed diamonds 4 m away; open diamonds 1 m away and open circles 0.1 m away from the vent center). (Modified from *Mar. Chem.*, **69**, 43–54 (2000), Wenzhöfer *et al.*, In situ microsensor studies of a hydrothermal vent at Milso (Greece), with permission from Elsevier Science.)

From microprofiles and continuous sensor readings at given positions a microcirculation pattern driven by the centrally out-flowing seep-water was resolved [57].

2.3 SENSITIVITY TO ANALYTE CONSUMPTION AND STIRRING

The measuring principle of an amperometric O_2 sensor is based on analyte consumption. Commonly applied macrosensors have current outputs in the order of 0.1–10 μA [13], which corresponds to an O_2 consumption rate by the sensors of 0.2–22 $\mu mol\, d^{-1}$. For a Clark-type microsensor this value is in the order of 20 pmol $O_2\, d^{-1}$ which is equivalent to the O_2 consumption of an individual dinoflagellate. The analyte consumption of O_2 sensors in itself rarely

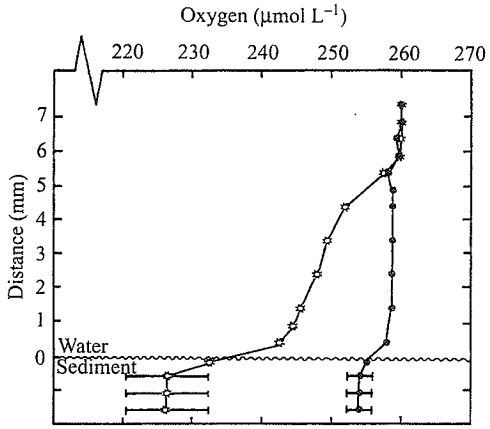

Figure 7. Apparent O_2 profiles as measured with two Clark-type O_2 microelectrodes having stirring sensitivities of 6% (✲) and 1%(●) respectively. The gradients are measured through a stirred 8 mm thick water film covering a layer of inert glass beads (no O_2 consumption). The observed gradients are solely due to a gradual decrease in flow velocities. (From Revsbech, N. P. R., *Limnol. Oceanogr.*, **34**, 474 (1989). Reproduced by permission of American Society of Limnology & Oceanography.)

poses a problem to measurements, and for respirometry the cathode size is usually scaled down below the expected O_2 consumption rate of the investigated object [58].

However, the fact that the sensor consumes the analyte, and thus requires a steady flux of analyte into the sensing tip, implies that the sensor signal will be affected by the transport of the analyte in the surrounding medium—the so-called 'stirring sensitivity' [59]. For interface studies the stirring sensitivity is a very important parameter, since the moving of a sensor tip from the free flowing water to the stagnant intersititial water of the sediments will cause a signal decrease solely due to the decrease in mass transport of oxygen (Figure 7). Stirring sensitivity is usually quantified as the percentage increase in sensor signal following the onset of vigorous agitation around a submerged sensor tip. This principle has recently been applied for the construction of a diffusivity sensor [60].

The stirring sensitivity of a Clark-type O_2 microsensor is largely determined by the sensor geometry and the diffusive path that O_2 must travel from the medium to reach the polarized catalytic surface (see also chapter 8). The path can be divided into two parts (Figure 8): (i) an internal part within the electrode (i.e. the distance from the sensor tip to the catalytic surface) and which is insensitive to stirring and (ii) an external part within the diffusion layer (DL) surrounding the sensor tip (Figure 8). The thickness of the DL will be a function of the water flow, as an increasing flow velocity will gradually erode the DL

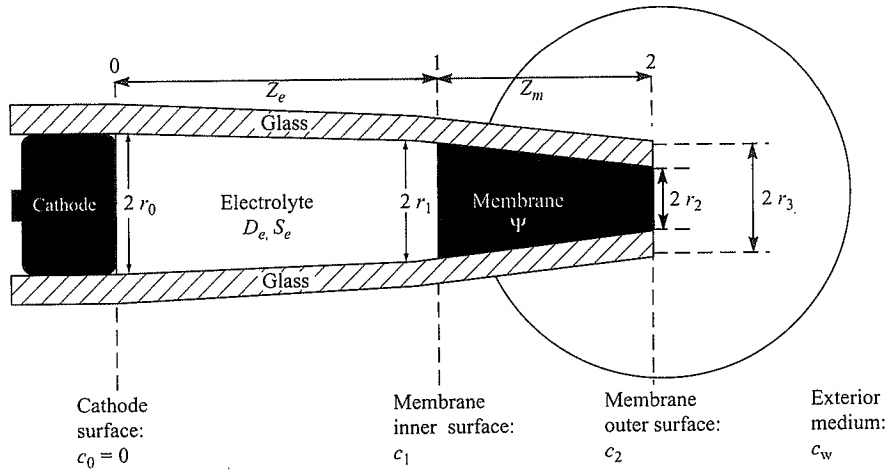

Figure 8. The tip of a Clark-type O_2 microelectrode including a hypothetical diffusion sphere (DL) outside the sensor tip

away. The analyte supply through the external medium is thus sensitive to stirring. The overall stirring sensitivity of the sensor is determined by the relative importance of the external and the internal paths in limiting O_2 flux to the sensing cathode. If the main restriction to O_2 flux is imposed within the sensor, then the electrode will be largely unaffected by stirring.

The model presented in section 2.2 describes the diffusive processes within the sensor. However, it assumes that the sensor is insensitive to stirring, i.e. the O_2 concentration at the sensor tip surface is equal to the concentration of the bulk water. The stirring effect can be included if we assume spherical oxygen gradients outside the sensor tip which replenish the O_2 consumed by the sensor (Figure 8). In stagnant water the O_2 distribution outside the sensor can be calculated by rearranging equation (1) into:

$$c_w = \mathrm{Si}S_w\left(\frac{Z_m}{r_2\Psi} + \frac{Z_e}{r_0 D_e S_e}\right)(\Phi\pi r_1)^{-1} \qquad (2)$$

where c_w is the O_2 concentration. The outside gradient can in theory be completely eroded away and the stirring sensitivity thereby becomes equivalent to the relative difference between O_2 concentration at the sensor surface and infinitely far away from the tip. Applying the O_2 concentration calculated from this relation and the oxygen flux as calculated from the electrode signal (Si), we can estimate the stirring sensitivity (ST) by using spherical diffusion equations [50]:

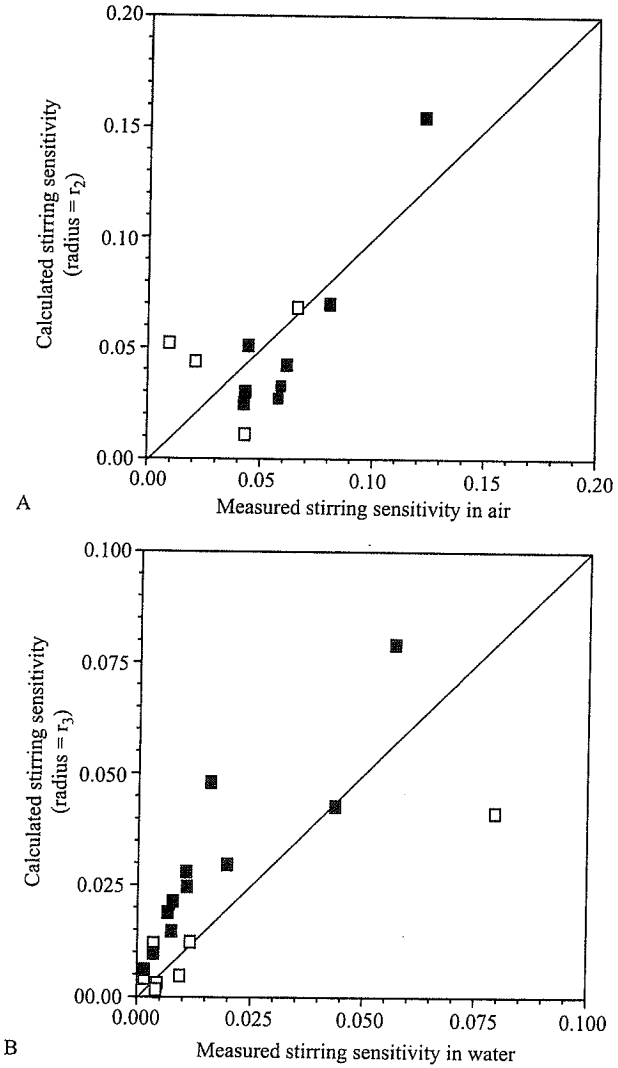

Figure 9. Calculated stirring sensitivity as a function of measured stirring sensitivity for 17 different Clark-type O_2 microelectrodes, in air (A) and water (B). Filled symbols represent sensors with a low r_3/r_2 ratio < 3 (please refer to Figure 8) and open symbols represent sensors with a high r_3/r_2 ratio > 3. r_2 and r_3 have been used for calculation of stirring sensitivity in (A) and (B), respectively.

$$ST = \frac{(c_w - c_2)}{c_w} = \frac{Si}{4r\pi D\Psi}\left(c_2 + \frac{Si}{4r\pi D\Psi}\right)^{-1} \quad (3)$$

where r equals the radius of the diffusing sphere (which is approximately equal to electrode opening) and c_w and c_2 are the O_2 concentrations in the exterior medium far away from the sensor and at the sensor surface, respectively.

It is not experimentally possible to erode the DL of a submerged electrode completely. However, by using the signal reading in air as being equivalent to recording under vigorously stirred conditions it was possible to compare theoretically and experimentally determined stirring sensitivities (Figure 9A). The comparison shows some scatter, but the points fall evenly around the 1:1 line. The poor correlation is probably a result of difficulties in determining the exact geometry of the various sensor tips under a microscope, and in measuring the correct temperature of the air-exposed electrode tip. If we thus assume that the stirring sensitivity corresponds to the erodible spherical concentration gradient outside the outer electrode diameter (instead of the inner electrode opening used in the previous model), we get a reasonable correlation between the calculated stirring sensitivity and the experimentally determined value (Figure 9B). The calculations can be used to identify the geometric parameters of importance for the stirring sensitivity and thereby for optimization of sensor design.

From the insight gained above it is clear that bare cathode-type O_2 microsensors or cathode sensors with a relatively thin membrane will have an extremely high stirring sensitivity. Cathode-type microsensors with stirring sensitivity as high as 50% have been applied in the laboratory [34]. However, by constructing microsensors with appropriate sensor geometry, membrane thickness, aspect ratio etc., cathode-type microsensors with stirring sensitivities $< 5\%$ have been made routinely [33,37]. The stirring sensitivities of Clark-type O_2 microsensors are usually around 1–2% but they can be made without any measurable stirring sensitivity if needed [40]. There is a trade-off between low stirring sensitivity and temporal resolution. A low stirring sensitivity is achieved by pulling the cathode back from the sensor opening but this will, however, also increase the response time of the sensor (see section 2.4.2).

Clark-type macroelectrodes being applied for measurements in water columns or within an enclosed water phase usually have significant stirring sensitivity in the order of 10–20% [13,61]. This is the result of large cathodes being applied with relatively thin membranes. In order to reduce this problem double membrane electrodes have been constructed [62]. However, in most commercial macro-probes, flow-through systems or stirred measuring chambers are mounted around the sensor tips in order to ensure insensitivity to the ambient water flow [15,63].

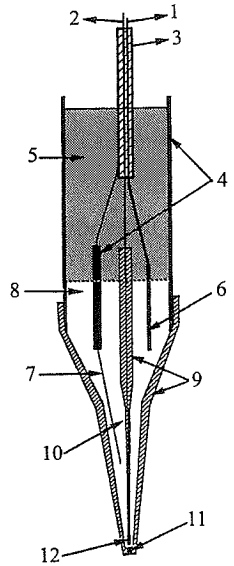

Figure 10. A Clark-type O_2 'mini'-electrode specially developed for fast, stirring-insensitive, measurements in water columns. Tip diameter is 30 μm. 1 = anode, 2 = cathode, 3 = ground, 4 = soda glass, 5 = epoxy resin, 6 = silver wire (anode), 7 = silver wire (guard cathode), 8 = 1.5 mol L^{-1} KCl, 9 = Schott 8533 glass, 10 = platinum wire (measuring cathode), 11 = silastic membrane, 12 = gold-plated cathode. (From Oldham, C., *Limnol. Oceanogr.*, **39**, 1959 (1994). Reproduced by permission of American Society of Limnology & Oceanography.)

The experience gained from O_2 microsensing at interfaces was recently adapted to a mini-CTD developed for studying fine-scale O_2 patches in water columns [22]. The O_2 sensor developed was in principle a Clark-type microelectrode, with a reinforced outer glass casing leading to an outer sensor tip diameter of 30 μm. The internal sensor hole, however, was only a few μm (Figure 10). Thereby the advantages of low stirring sensitivity (a few %) and fast response time (around 0.15 s for 90% response) characteristic of microsensors was combined with a rugged design [22]. Owing to the fast response and no requirement for a constant water flow over the sensor surface the O_2 'mini'-sensor could be incorporated into a free – ascending CTD instrument, measuring high resolution water column profiles of temperature, and O_2 [22]. A similar sensor, with slight modifications resulting in better long-term stability, was developed for O_2 measurements during deep-sea deployments of benthic chamber landers [64].

2.4 SPATIAL AND TEMPORAL RESOLUTION

As already mentioned in section 1.1.2 discussions of spatial and temporal resolution of microsensors are mostly relevant for studies at interfaces or within the sediment matrix. Necessary sensor characteristics for water column measurements can practically always be met by standard O_2 microsensors, because of their small size, low stirring sensitivity and fast response.

2.4.1 Spatial Resolution

Microsensors do not change the O_2 concentration significantly at the measuring site because of their very limited O_2 consumption rate. Therefore, the spatial resolution by which a steady state microgradient can be resolved is in principle set by the diameter of the sensor tip. As a general rule we assume that the spatial resolution of a sensor is in the order of two times the outside tip diameter. Cathode-type microsensors can be made extremely small with tip diameters below 1 μm [32], while the tip diameter of Clark-type microsensors is usually around 1–10 μm [40]. For most practical purposes such spatial resolution is more than sufficient to resolve the concentration gradients across interfaces within aquatic environments [16]. In most cases mechanical problems related to electrode positioning (using manual or motor-controlled micromanipulators) or to physical disturbances within the environment are the factors limiting the spatial resolution, rather than the tip size of the microsensors. Needle-like cathode sensors with tip diameters of 600–800 μm have a correspondingly lower resolution and their high O_2 consumption rates may cause local distortion of the O_2 gradient.

A practical problem related to sensor size that should be mentioned is that very thin sensors are fragile. In many sediments (and especially on solid surfaces) this has to be taken into account. Years of *in situ* application of microsensors has taught us that tip sizes in the order of 10–25 μm are sufficiently rigid to survive microprofiling through the oxic zone of normal coastal sediments. Another practical concern is the extent to which microsensors mechanically disturb the structure of the sediment as they penetrate. This is still an open question, although repeated measurements at the same location with microsensors usually reveal only slight differences between the first and the subsequent profiles, indicating that any mechanical disturbance is of minor importance. Another study concluded that microprofiles resolved by needle electrodes (tip diameter 0.7 mm) and cathode microelectrodes (tip diameter 2–10 μm) were very 'similar' and that no 'significant difference' between such profiles could be observed at a spatial resolution of 0.5 mm [38]. The study was performed in a silty sediment with O_2 penetration depths of approximately 10 mm. Any potential effect will probably depend on the sediment characteristics and the slope of the O_2 gradients, and it still remains

to be shown to what extent sensor dimensions affect measured porewater profiles.

The high spatial resolution that can be obtained with O_2 microelectrodes has allowed studies on O_2 concentration gradients towards or within meiofauna individuals and marine aggregates (marine snow) [27,65,66]. For 'on site' or laboratory-based studies within microbiota or in symbiosis it has to be recognized that microsensor techniques are invasive. Phobic responses to mechanical disturbances or related to penetration of tissue cannot always be neglected [27], and are a matter of concern in physiological studies [67].

2.4.2 Temporal Resolution

After experiencing an abrupt change in the O_2 concentration, the signal of a microelectrode follows an exponential response curve [32]. It is therefore difficult to evaluate the exact time period required for a 100% sensor response. The response times given for various microsensors are therefore usually the 90% response time, i.e. the time required to reach 90% of the total signal change, after an abrupt change in the O_2 concentration. The response time of a sensor is due to the time it takes diffusion to establish a new steady-state gradient through the sensor tip following a change in partial pressure. The response time (t_{90}) is thereby a function of the transport coefficient (D and/or Ψ) and the distance from the bulk water to the sensing cathode. As the transport both in the electrolyte and in the membrane material may present the rate limiting transport, the response time can be estimated by $t_{90} = (K_e Z_e^2 D^{-1}) + (K_m Z_m^2 s_m \Psi^{-1})$ where K_e and K_m are constants and s_m the solubility in the membranes [49]. Most membrane materials have O_2 permeabilities of the same order of magnitude as that of stagnant water and seldom pose a limit to the response time of a sensor. However, the O_2 solubility in some membranes, e.g. the silicone frequently used for Clark-type O_2 sensors, is much higher than the solubility in water. The membrane thus has to be filled up before a steady state gradient can be reached, which will increase the response time, while improving the selectivity for the many hydrophilic ions/compounds of the medium which may interfere with measurements. In all cases the response time is proportional to Z^2, which makes the distance between the cathode and the exterior medium the most critical parameter. Bare cathode-type sensors are therefore extremely fast (a few μs), while membrane-coated cathodes or Clark-type sensors are somewhat slower (see Table 1). As mentioned above, there is a trade-off between stirring sensitivity and response time of microsensors, and the optimal sensor for a given application has to be evaluated in that context. The geometry of a Clark-type O_2 microsensor can be optimized so that stirring sensitivities are kept below 1% and the 90% response time is below 0.5 s. This, however, requires a very skilful constructor.

2.4.3 Case Study 1: Thickness and Stability of the Benthic Diffusive Boundary Layer (DBL)

Although the existence of the DBL had been known for many years [68], the physical reality and its significance first became apparent when microelectrodes were applied to studies of benthic interfaces [69]. *In situ* application of membrane-coated cathode sensors combined with high resolution video recording demonstrated a signal decrease, significantly larger than the 3–5% stirring sensitivity of the applied sensors, just above the sediment surface [70]. This was used to indicate the existence of a DBL covering marine sediments, and the thickness above deep sea sediments was estimated to be of the order of 0.5–1.5 mm [70]. These values were later refined by high resolution microsensor measurements both in coastal and deep sea sediments [71,72]. In laboratory studies it was shown that the thickness of the DBL was primarily a function of the water flow velocity above the sediment and the sediment roughness (Figure 11) [26,69], as might be theoretically expected.

At the scale of a microsensor tip the sediment–water interface is usually not a planar surface but a landscape with 'mountains' and 'valleys'. A detailed 3D mapping demonstrated how the DBL covered the sediment surface like a

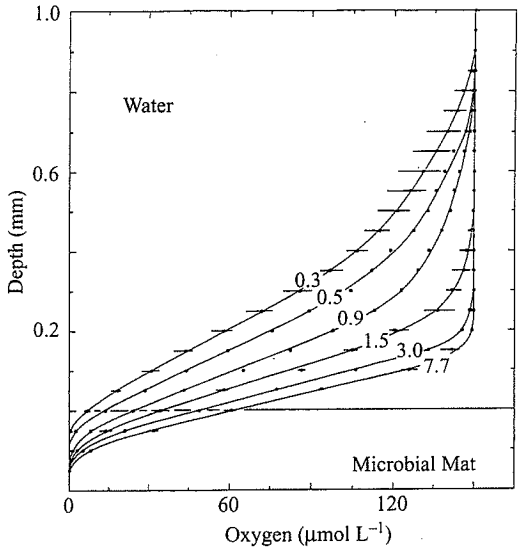

Figure 11. Oxygen microprofiles measured above a cyanobacterial mat at six different free-flow velocities ranging from 0.3 to 7.7 cm s^{-1} (indicated in figure). Depth 0.0 is equivalent to the mat surface and small horizontal bars indicate the standard deviation of four measurements (only shown for velocities of 0.3, 1.5 and 7.7 cm s^{-1}). (From Jorgensen, B. B., and Des Marias. D. J., *Limnol. Oceanogr.*, **35**, 1343 (1990). Reproduced by permission of American Society of Limnology & Oceanography.)

'carpet' being thinner on the upstream sides and thicker on the lee side of small mounts [26] (Figure 12). This shows that in the case of rough microtopography a geometric correction term has to be included to calculate accurate fluxes from vertical profiles, as the assumption of planar diffusion is invalid and since the profiles usually are not perpendicular to the DBL and sediment surfaces [26]. Continuous recordings of the O_2 concentration at given depths within the DBL have also demonstrated a fluctuating signal with a characteristic pattern [71]. The amplitude of the fluctuations increased in the upper part of the DBL only to decrease together with the frequency of the O_2 fluctuations as the sediment surface was approached. Increasing flow velocities of the overlying water reduced the amplitude of the oscillations but increased their frequency (Figure 13). These phenomena were interpreted as eddy intrusions from the turbulent phase above the DBL which penetrate down into the linear flow of the DBL [71,73]. At high flow velocities, the fluctuation frequency was as fast as the response time of the applied sensors [71]. The frequency and amplitudes of these fluctuations measured at high flow velocities are therefore probably underestimated in these studies. For more detailed studies on the O_2 fluctuations, faster electrodes (e.g. bare cathode sensors) could be applied, although their higher stirring sensitivity could lead to ambiguous results.

The linear O_2 concentration gradients within the DBL (Figure 11) are often used to calculate the net O_2 uptake (or release) of sediments [74]. The calculations are based on Fick's first law of diffusion: $J = D\,dc/dz$, where J is the flux, D the diffusion coefficient, c the O_2 concentration and z the depth [50]. An advantage of this approach is a well-established transport coefficient, the molecular diffusion coefficient for oxygen, within the DBL. It is, however, still unclear to what extent intrusions from the overlying water into the DBL affects the mass-transport within the DBL. Flux estimates within the sediment require an empirical determination of the transport coefficient which incorporates the molecular diffusion coefficient, porosity, and tortuosity factors [75,76]. The main problem for *in situ* studies of the DBL is to determine the exact position of the sediment surface. Recently, a reflection-based fiber optical sensor was used to determine the exact position of the sediment surface [77]. Such a sensor could easily be fixed on a microelectrode for simultaneous surface detection. Other commonly applied techniques for determining the position of the sediment surface are resistivity probes [75,78] or changes in the slope of the concentration profiles which indicate the reduced transport coefficients of sediments [79].

In section 2.4.1 we discussed the physical disturbance which could be associated with measurements in sediments or tissue. It was previously anticipated that the small tip diameter of O_2 microsensors allowed measurements to be made within the DBL without any disturbance [26,71]. However, detailed 3D mapping of the DBL structure, with a microsensor coming from below, up through the sediment matrix, revealed a major distortion of the DBL structure

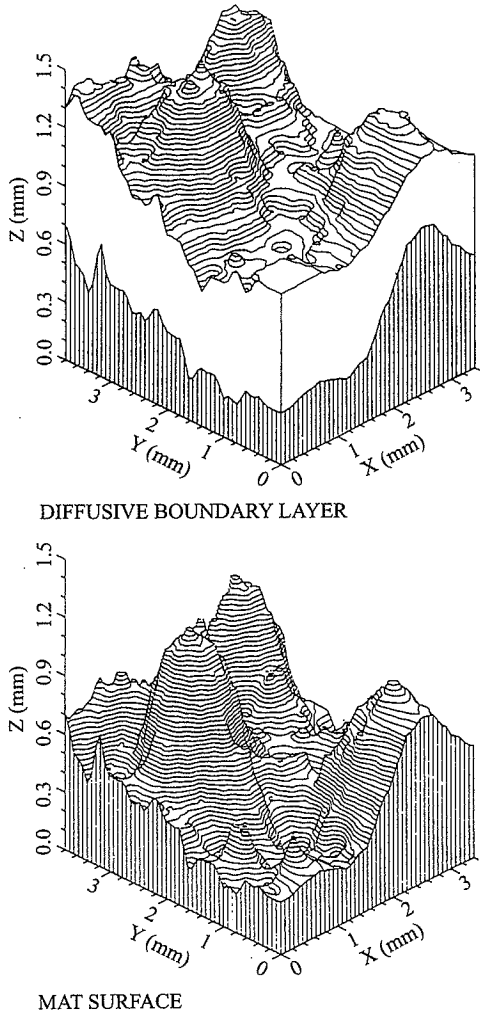

Figure 12. Three-dimensional plot of the microtopography of a microbial mat and the overlying DBL, measured by multiple insertions of a microelectrode. A structure of 0.5–1.0 mm protruding from the investigated area (3.6 mm along the X-axis and 3.8 mm along the Y-axis) caused smoothened deflections of the DBL. The Z-axis has a maximum value of 1.5 mm in both panels. The flow was in the direction of the positive Y-axis and the free flow velocity was 0.4 cm s^{-1}. (From Jorgensen, B. B., and Des Marias. D. J., *Limnol. Oceanogr.*, **35**, 1343 (1990). Reproduced by permission of American Society of Limnology & Oceanography.)

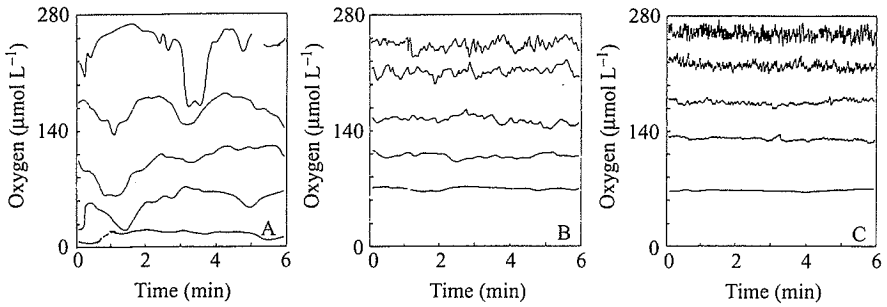

Figure 13. Continuous recordings of the O_2 concentrations at various distances above and below a microbial mat surface at three different flow velocities: (A) 0.3, (B) 1.3 and (C) 9.3 cm s^{-1}. The data were recorded at the following distances in relation to the mat surface: (A) 0.50, 0.30, 0.10, 0.00 , and −0.10 mm; (negative below mat surface); (B) 0.30, 0.20, 0.10, 0.00, and −0.10 mm; (C) 0.10, 0.05, 0.00, −0.05 , and −0.20 mm. The fluctuations mirror the effect of eddies in the flowing water that interact with the O_2 concentrations within the DBL. (Redrawn from Gundersen, J. K., and Jorgensen, B.B., *Nature*, **345**, 604 (1990). With permission.)

around a microsensor tip coming from above (Figure 14) [80]. The DBL immediately below the sensor tip was compressed by 25–45 % and previous estimates of the DBL thickness with microsensors were most likely underestimated correspondingly. The mechanism behind this effect is still not clear, but is most likely associated with pressure differences due to acceleration and deceleration of water flow around the electrode shaft, which is placed in a vertical velocity gradient [80]. The quantitative importance of the effect is mainly a function of the water flow velocity and the sensor geometry. Thick and stubby sensors impose a larger problem, however, even very thin and elongated sensors (< 10 µm thick) show clear evidence of DBL depression. Over very irregular surfaces the effect may to some extent be masked by interaction between flowing water, the sensor, and the microtopography [81].

2.4.4 Case Study 2: Gross Photosynthesis Measurements

Studies on benthic photosynthesis require microsensors with high temporal and spatial resolution. Steady state microprofiles with a spatial resolution of 50–100 µm have often been used to estimate the net O_2 export out of photosynthetic communities [82,83]. However, using the co-called 'light/dark shift technique' it is also possible to quantify the gross photosynthetic activity at a relatively high spatial resolution [84,85]. Using this technique the gross photosynthesis is calculated from the initial decrease in oxygen concentration at a given position after eclipse of the light source, assuming: (I) a steady-state O_2 distribution in the community before darkening, (II) an identical

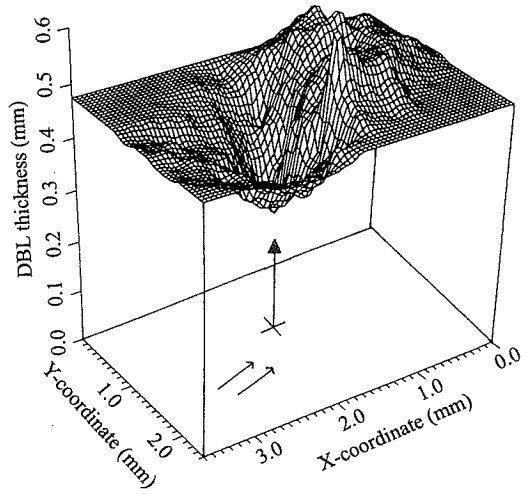

Figure 14. The disturbed DBL structure following the placement of a microelectrode (tip size 8 µm) at a depth position of 0.3 mm (indicated by large arrowhead). Prior to insertion the DBL was flat as was the benthic interface itself. Small arrows indicate the flow direction (flow velocity was approximately 3 cm s^{-1}). The sediment surface is at a depth position of 0.0 mm. (From Glud *et al.*, *Limnol. Oceanogr.*, **39**, 462 (1994). Reproduced by permission of American Society of Limnology & Oceanography.)

O_2 consumption before and during the light–dark shift, and (III) constant O_2 gradients within the community during the dark incubation. It has been demonstrated that assumptions (I) and (II) can be fulfilled in benthic photosynthetic communities but that (III) requires fast sampling during a short eclipse period so that the absolutely initial decrease in O_2 concentration is used for the calculation [85,86].

Within a cyanobacteria-dominated system, O_2 concentrations during light/dark cycles were recorded at a total of 22 depth horizons at a temporal resolution of 100 ms. From these data the O_2 microprofiles in light and after 1, 2, and 3.8 s of darkness were calculated (Figure 15A). The continuous recordings at four sediment depths are shown in Figure 15B. They clearly demonstrate that the rate of O_2 decrease changes during the dark incubation. In other words the O_2 concentration gradients changed after the eclipse of the light source (assumption (III) is not fulfilled). The gross photosynthetic rate measured after 1.1 and 2.6 s of darkness (Figure 16) show that the depth distribution of the measured activity widens out, so that peak activities were underestimated and the low activities are overestimated with longer incubation time. The depth-integrated activity, however, remained constant within a dark incubation period of 4 s (Figure 16B) [85,86]. The observed effect is the result of a net O_2 diffusion along the concentration gradients during the dark incubation, and

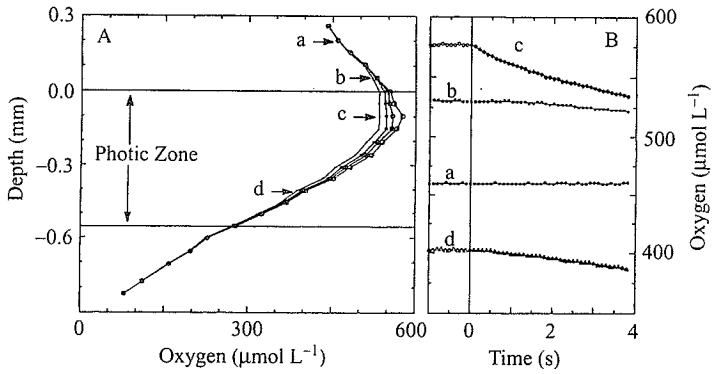

Figure 15. Oxygen distributions immediately above and within a cyanobacteria-dominated microbial mat during a light–dark shift. The depth of 0.00 mm indicates the mat surface, while position −0.55 mm indicates the lower boundary of the photic zone. The constructed profiles were obtained in light (large open circles), 1 s after darkening (large filled circles), 2 s after darkening (medium filled circles) and 3.8 s after darkening (small filled circles). Letters in the left panel indicate the positions of the continuous recordings presented in the right panel. (From Glud, R.N., *et al.*, *J. Phycol.*, **28**, 51 (1992). With permission.)

demonstrate that, in order to measure the true distribution of photosynthesis, the O_2 decrease immediately after onset of darkness has to be obtained.

A rough estimate of the spatial resolution obtainable in gross photosynthetic measurements can be deduced from the following equation: $\delta = (2Dt)^{0.5}$; where δ is the distance O_2 molecules move away from a given depth horizon in the time interval t, given a diffusion coefficient of D [87]. This means that within a period of 1 s at 20 °C ($D = 2.0 \times 10^{-9}$ m^2 s^{-1}), 32% of the O_2 molecules would move more than 63 μm [84]. Gross photosynthetic measurements in two adjacent layers are therefore not independent if the applied dark period is too long compared with the specified spatial resolution. For measurements of gross photosynthesis it is therefore crucial to apply fast sensors (and measuring instruments) [85,86].

2.5 HYDROSTATIC PRESSURE EFFECTS

2.5.1 General Discussion

Interface studies or *in situ* respirometry are usually performed at constant but possibly elevated hydrostatic pressures, while water column measurements are conducted through a hydrostatic pressure gradient. Proper calibration of the sensor signals requires a thorough understanding of how hydrostatic pressure affects the electrode signal.

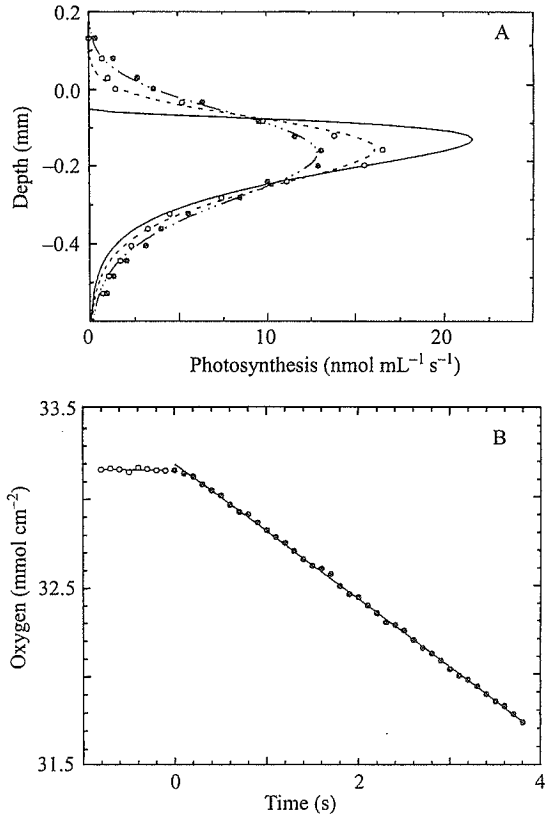

Figure 16. (A) Measured and simulated microprofiles of gross photosynthesis in a cyanobacterial microbial mat. Data recorded after 1.1 (open circles) and 2.6 s (filled circles) of darkness are displayed together with the equivalent simulated profiles, the simulated activity profile after 0.0 s is shown as a continuous curve (for the simulation procedure, refer to the original manuscript). (B) The depth-integrated O_2 concentration within the photic zone during a light–dark shift (time 0.0 s). The linear decrease indicates a constant O_2 consumption rate from the onset of darkness. Open symbols were recorded in light, while the filled symbols were recorded in darkness. (From Glud, R.N., *et al.*, *J. Phycol.*, **28**, 51 (1992). With permission.)

For understanding the effects of pressure on electrodes it is important to realize that membrane-coated sensors respond to the partial pressures (actually the fugacity of O_2), rather than O_2 concentrations. Various parameters of importance for the signal of an O_2 electrode will change with increasing hydrostatic pressure: (I) the O_2 partial pressure (fugacity), (II) the membrane permeability, (III) diffusion coefficient of O_2, (IV) the activation volumes at the cathode and anode.

Since the dissolved O_2 is generally not in direct equilibrium with air at any given water depth the partial pressure of O_2 is not defined. It is therefore more appropriate to use the term O_2 fugacity. The O_2 fugacity change (f) as a function of hydrostatic pressure is described by the following equation:

$$f = f_0 \exp(v\Delta P/RT) \quad (4)$$

where f_0 is the fugacity at the water column surface, v is the partial molar volume of O_2, ΔP is the hydrostatic pressure change, R is the gas constant, and T is the absolute temperature [88]. A laboratory study obtained an excellent match between the output of a DPX-coated cathode microelectrode exposed to hydrostatic pressures between 0.1 and 60 MPa (1–600 bar) and equation (4) (Figure 17) [89]. This indicates that for that sensor type the O_2 permeability of the DPX membrane was insensitive to hydrostatic pressure.

For Clark-type macrosensors it is a common observation that the sensor signal decreases with increasing hydrostatic pressure, and the effect is ascribed to decreasing permeability of the sensor membrane [90–92]. In order to avoid disruption of Clark-type O_2 sensors during deep-sea application (or pressure testing) the electrolyte is pressure compensated over a flexible membrane [44]. The Clark-type microsensor exhibits a close to linear signal decrease with increasing hydrostatic pressure (Figure 18A), as was found for macrosensors

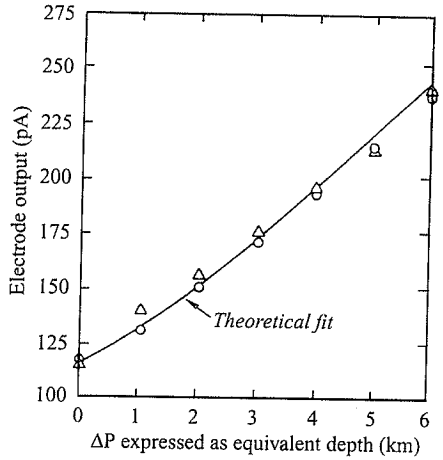

Figure 17. The hydrostatic pressure response of a cathode-type O_2 microelectrode equipped with a DPX membrane. Two replicate measurements were performed in two subsequent pressure cycles (circles and triangles). The output signal is in picoamperes (p_A). The theoretical response as predicted by Equation (2) is indicated by a solid line. (An erratum has later made a slight correction to the theoretical fit, but without importance in the present context.) (Reproduced from *Deep-Sea Res.*, **34**, Reimers, C.E., 2019 (1987), with permission from Elsevier Science.)

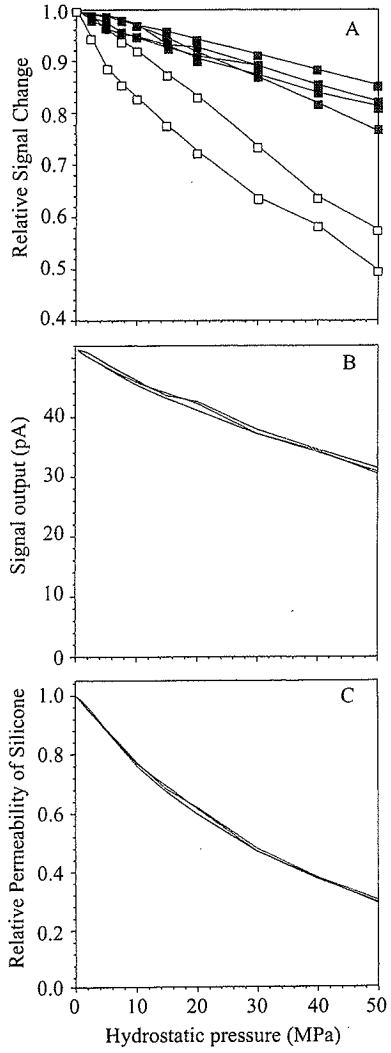

Figure 18. (A) Changes in the relative signal of six different Clark-type O_2 microelectrodes with increasing hydrostatic pressure. The two most pressure sensitive sensors also had the longest silicone membrane. (B) The response of a microelectrode (in picoamperes during three replicate pressure cycles and (C) the decrease in silicone permeability that was required in order to explain the observed sensor response solely by permeability changes

Generally, we observe that microelectrodes with a relatively thick silicone membrane show a stronger signal decrease with pressure. This suggests that the effect is related to a decrease in membrane permeability, which exceeds the effect of the partial pressure increase. Hysteresis effects are seldom seen and repeated pressure cycles reveal very reproducible sensor responses (Figure 18B). The change in membrane permeability that is required to give the observed sensor response can be calculated by applying the model described in section 2.2 (Figure 18C). The estimated permeability decreases exponentially with increasing pressure. The pressure at which the permeability is 50% of the value at atmospheric pressure is around 40 MPa (400 bar) for all sensors tested, although the absolute permeability differs amongst electrodes. This is likely to be related to variability in the physical characteristics of the silicone membranes (aging, hydration etc.) and the fact that the geometry of a given sensor is difficult to measure exactly. When applying a Clark-type O_2 microsensor under variable hydrostatic pressure, it is therefore recommended to perform an empirical determination of pressure response of each sensor and to include the results in the calibration procedure. For interface studies or respirometry at elevated hydrostatic pressures the sensor calibration should preferably be performed *in situ* [44,72]. Measurements in pressure chambers have shown that the zero current of the Clark-type O_2 microsensors is independent of hydrostatic pressure (data not shown). For commercially available macrosensors, standardized production procedures ensure that the empirical relationship describing hydrostatic pressure effects on the sensor signal can be incorporated in the calibration software which is usually purchased along with the sensors [92,93].

The diffusion coefficients decrease along with the viscosity at elevated hydrostatic pressures. However, the effect is minimal (4% for ΔP of 60 MPa), and does not have a major effect on the sensor output. For a commercially available O_2 macroelectrode the hydrostatic pressure effects on activation volumes were calculated to be of minor importance [91], and a study concluded that change in membrane permeability was the controlling factor for the electrode signal at hydrostatic pressures up to at least 100 MPa [91].

2.5.2 Case Study 3: Deep-sea Measurements (*In Situ* and On Site)

Deep-sea interface studies are performed at constant but very high hydrostatic pressures. However, if the electrodes are protected by a pressure compensating system between electrolyte and ambient water, they remain fully functional [44]. Figure 19A presents O_2 profiles measured over the sediment water interface at stations along a depth transect in the SE Atlantic [72]. The profiles reflect the gradual increase in O_2 penetration depth as a result of the reduced sedimentation of organic material in deep-sea environments (and to much lesser extent an increase in the O_2 concentration of the bottom water). Owing to the extreme O_2 penetration depth at the deepest investigated site the microelectrode

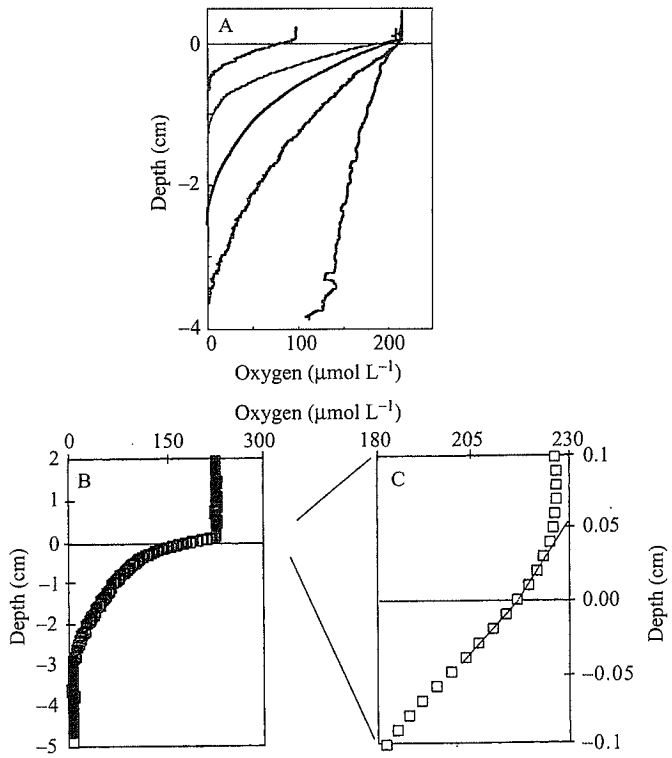

Figure 19. (A) *In situ* O_2 microprofiles obtained at a spatial resolution of 100 μm along a depth transect in the SE Atlantic. Profiles show a gradual increase in O_2 penetration with the water depth: 600, 1743, 1960, 3100 and 4986 m. (B) The profile obtained at 3100 m with an enlargement of the sediment water interface (horizontal line). (Reprinted from *Deep-Sea Res.*, **41**, Glud *et al.*, 1767 (1994), with permission from Elsevier Science.)

broke before reaching the anoxic horizon. Figure 19B presents a magnified view of the interface measurements performed at 3100 m water depth and demonstrates the high spatial resolution required to resolve the O_2 gradients within the DBL. In order to obtain complete microprofiles and high resolution DBL measurements simultaneously, it may be necessary to equip the instrument package with a combination of large robust sensors (for deep profiles) and thin sensors for the DBL measurements [94]. In order to resolve the very small concentration change across the DBL in the deep sea, it is necessary that the applied sensors have practically no stirring sensitivity (see section 2.3).

Parallel *in situ* and on site measurements have demonstrated a significant change in the surficial O_2 distribution after recovery of deep-sea sediment cores.

For instance, the 'on site' O_2 penetration depth was only 20% of the *in situ* value while the calculated sediment O_2 uptake was 3.5 times higher in the laboratory as compared with *in situ* [72]. The effects are probably related to transient heating during core recovery and pressure-release effects on specially adapted meio- and microfauna [72,95]. These findings emphasize the need for *in situ* O_2 measurements to obtain realistic estimates of the benthic distribution and exchange of O_2 in the deep sea.

2.6 STABILITY, LIFETIME, AND INTERFERENCES

It is difficult to give any absolute values for the stability and lifetime of various O_2 microelectrodes, since they are very much dependent upon the environmental conditions. Under laboratory conditions [32] it has been found that for cathode-type sensors the signal at air saturation and in anoxia varied by 9.3% and 1.3%, respectively ($n = 7$) over a 30 d period. Also under laboratory conditions, we have measured the average drift in the air saturation signal of Clark-type O_2 microsensors to be in the order of 2% d^{-1} ($n = 25$). However, this drift may to some extent be due to small changes in temperature and air pressure. As estimated from equation (1) a signal change of 2% could be the result of a minor temperature change of < 1 °C. It is often observed that after polarization the sensor signal as well as the zero-current show an initial decrease. This is associated with an initial reduction of O_2 dissolved in the electrolyte, and it is therefore recommended to keep Clark-type O_2 sensors polarized for a few hours prior to application. The most common reason for a significant signal drift during measurements is malfunctioning or leaky membranes [59]. The lifetime of both cathode-type and Clark-type O_2 microelectrodes is usually in the order of months to years unless they are mechanically damaged or 'poisoned' by interfering compounds [96].

The ion-permeable membrane-coated O_2 cathode sensor, which has an external reference is an open system, and solutes in the environment can therefore potentially interfere with the measuring circuit. Cathode sensors can be poisoned by ions, in particular, Ca^{2+} and Mg^{2+}, presumably due to precipitation of hydroxides and carbonates at the cathode surface and in the membrane [16,32]. This process is stimulated by the alkaline microenvironment generated by the reduction of O_2 to OH^-. Dissolved organic material may in a similar manner change the cathode surface and the structure of the membrane. The result is a non-linear and a drifting calibration curve. For these reasons cathode sensors with hydrophilic membrane coatings are not optimal for *in situ* O_2 measurements. To our knowledge no detailed studies on the interference of various agents on hydrophilic-coated cathode sensors have been performed. However, for *in situ* measurements such sensors are gradually being replaced by Clark-type microelectrodes (or microoptodes—see below).

For microsensors with hydrophobic membranes the only major interfering agent is H_2S, which can pass the gas-permeable membrane and interfere with the electrochemical reactions of the sensor. The result is usually an increase and drift of the signal. Precipitation of various sulfur–metal complexes within the sensor tip, which change the catalytic surface as well as the membrane structure, can be observed [59]. In the worst case H_2S-poisoned sensors lose their sensitivity to O_2. The mechanism of H_2S poisoning of microelectrodes, however, is very complex and not fully understood [59]. It is noticeable that for cathode-type sensors it has been observed that partly poisoned electrodes, with a reduced sensitivity to O_2, become insensitive to H_2S and can subsequently be used for O_2 measurements within an H_2S gradient [20]. The reason for this behavior is still unclear. It is, however, important to note that, for most relevant habitats, the H_2S and O_2 containing horizons are well separated spatially.

A sulfide-resistant macro-O_2 electrode based on a gold cathode, and with an alkaline sodium sulfide solution has been developed [59]. The anode is Ag/Ag_2S, whose potential is approximately −0.7 V. The cathode is kept at a fixed potential of −0.1 V versus this reference electrode. The principle has been tested on a microscale; the lifetime of such sensors is limited (approximately 1 week) owing to precipitation of S^0 at the sensor tip [56]. In general, interfering agents are a minor problem for *in situ* application of Clark-type O_2 microelectrodes.

3 OPTICAL MICROSENSORS (MICROOPTODES)

Recently a new generation of microsensors for *in situ* O_2 measurements has been introduced to aquatic science. The sensors are not based on any electrochemical principle, but take advantage of an optochemical technique. The so-called microoptodes were developed by minaturizing and optimizing sensors that previously had been applied in other fields of science [97–99]. Such microsensors were recently tested for their potential for *in situ* applications [100]. Needle-supported minioptodes (diameter 1–3 mm), and macrooptodes applying the same principles, have been developed for applications in water columns, coarse sediments and for measuring very deep O_2 profiles [94,101,102]. The development of optodes, and associated electronics for *in situ* applications in aquatic environments, is still in its early stage. So far only measuring systems where the fluorescence intensity is used as analyte-dependent parameter have been realized. However, fluorescent lifetime-based sensing schemes have great potential and will probably lead to further advances in coming years (see Section 3.4).

3.1 CONSTRUCTION AND FUNCTION

The basic principle of O_2 microoptodes is dynamic fluorescence quenching [103]. In the absence of O_2 the fluorophore absorbs light at a given wavelength

and releases the absorbed energy by emitting fluorescence with a defined intensity and lifetime. However, in the presence of O_2, quenching of the fluorophore results in a decrease of the fluorescence light intensity as well as in the fluorescence lifetime.

The first microoptode was based on a ruthenium complex (ruthenium(II) tris-4–7–diphenyl-1,10–phenanthroline perchlorate) $Ru(diph)_3$, which was dissolved in polystyrene (PS) [104] (Figure 20). Titanium dioxide particles (diameter 1 μm) were added to the indicator–polymer mixture in order to enhance the mechanical stability and to provide more efficient scattering of the emitted light. An optical silica fiber with an outer diameter of 140 μm was tapered to a final diameter of 30 μm by heating. Subsequently the fiber tip was dip-coated with the indicator–matrix cocktail. After evaporation of all solvent (approximately 24 h), an additional layer of black silicone was coated onto the sensor tip in order to shield out ambient and backscattered light during measurements. A shielding is also required in order to avoid stimulation of any potential phototrophic activity in the investigated communities. The applied fluorophore has a large Stoke shift with an optimal absorption around 450 nm and an emission wavelength of 610 nm. This ensures that relatively cheap glass filters can be applied in the measuring set-up. The shaft was mechanically supported by a needle or by a glass capillary, and the tip diameter was approximately 40 μm (Figure 20). Physically the tip diameter could be made smaller, but this resulted in unacceptably low signal levels [104].

Besides the $Ru(diph)_3$–PS reactive layer, numerous other combinations of fluorophore and immobilization materials have been tested for their potential use in macro- and microoptodes [105–108]. Different chemically reactive layers have various advantages in relation to stability, response time, and sensitivity range, and selecting the optimal combination for a given task is often a trade-off between the various characteristics of the fluorophore and the

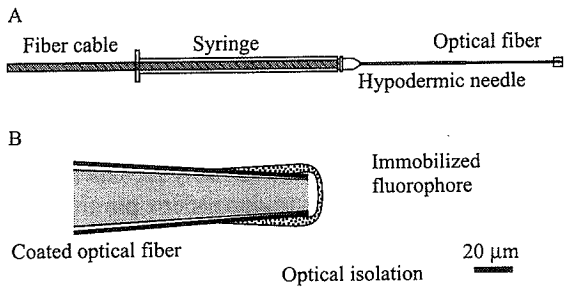

Figure 20. (A) Schematic presentation of an intensity based microoptode with an optical insulation layer. (B) Enlargement of the sensor tip (From Klimant *et al.*, *Limnol. Oceanogr.*, **40**, 1159 (1995). Reproduced by permission of American Society of Limnology & Oceanography.)

immobilization material [108]. The following criteria should in general be met by fluorophores and immobilization materials applied for intensity-based microoptodes: (I) the fluorophore should be excitable by a light emitting diode (LED), (II) the fluorophore must be sufficiently photostable, (III) the fluorophore should have a relatively large Stoke shift, (IV) the fluorophore should be non-soluble in water to ensure minimal dye leaching, (V) the fluorophore should be soluble in the hydrophobic polymer used for immobilization, (VI) O_2 should be highly soluble in the immobilization material, (VII) the immobilization material should be mechanically stable under the measuring conditions and adhere well to the fiber. Soft polymers such as silicone, plasticized poly(vinyl cloride) (PVC), or cellulose derivates do not adhere very well and are easily mechanically damaged during sensor application. Mechanically stable hydrophobic materials such as PS or poly(methyl methacylate) (PMMA) appear to be better suited as immobilization materials [108]. Recently sol–gels (ormosils) have proven to be robust and stable as immobilization materials [109]. Sol–gels are condensed silica alkoxides, which form a highly permeable non-crystalline structure. The addition of organic-substituted precursors may increase the flexibility and lower the brittleness of the material [110]. Table 2 compiles the characteristics of some chemically reactive layers that have been tested for use in microoptodes.

Table 2. Composition and selected properties for sensing material, which have been tested for microoptodes (modified from Klimant *et al.*, 1997)

Fluorophore (luminophore)/ Immobilization material	Signal	Response time (t_{90})	Sensitivity*	Excitation/ Emission light (nm)	Photostability/ Mechanical stability
$Ru(diph)_3$ / PS†	very high	< 2 s	22 %	450/600	very good/ very good
$Ru(diph)_3$ / PVC	very high	< 200 ms	59 %	450/600	poor /poor
Pt-OEP‡/PS	high	< 2 s	80 %	400 and 535/640	moderate/very good
Pt-OEP/PMMA§	high	< 5 s	35 %	400 and 535/640	moderate/good
Pt-OEKP¶/PS	moderate	< 2 s	75 %	400 and 592/760	good/very good
Pd-OEP**/PS	moderate	< 2 s	98 %	400 and 545/670	poor/very good

* Signal decrease following transfer from nitrogen to air.
† Polystyrene.
‡ Platinum(II)-octaethylporphyrin.
§ Poly (methyl-methacrylate).
¶ Platinum(II)-octaethylketoporphyrin.
** Palladium(II)-octaethylporphyrin.

$Ru(diph)_3$ is a fluorophore which meets all of the criteria mentioned above and has been selected by various research groups as the optimal indicator for *in situ* application [94,100,101,111]. As immobilization materials, both PS and sol-gels have proven to be reliable, and have been applied for *in situ* optode measurements [100,101].

3.2 CALIBRATION

The signal of optodes decreases non-linearly with increasing oxygen concentration, in contrast to oxygen electrodes (Figure 21). For an ideal dissolved fluorophore the calibration curve can be linearized using the Stern–Volmer equation [112]:

$$\frac{I_0}{I} = 1 + k_{sv}c \tag{5}$$

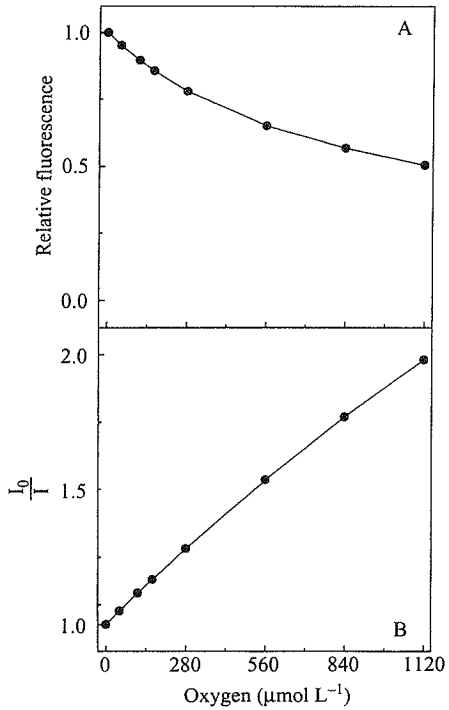

Figure 21. The calibration curve of an $Ru(diph)_3$ – PS – based microoptode (A) and the corresponding Stern–Volmer plot (B). (From Klimant *et al.*, *Limnol. Oceanogr.*, **40**, 1159 (1995). Reproduced by permission of American Society of Limnology & Oceanography.)

where I_0 and I are the fluorescence intensity in the absence and presence of oxygen, respectively, c is the oxygen concentration in the solution and k_{SV} the quenching coefficient. However, in reality O_2-sensitive fluorophores, which are dissolved in a solid matrix, exhibit non-linear Stern–Volmer calibration curves. A general calibration equation based on a two-site O_2 quenching model, which accounts for the non-ideal behavior of immobilized fluorophores, has been suggested [113]. The equation is, however, relatively complex and requires multiple calibration points, so for most practical applications a modified Stern–Volmer equation (which adequately describes the calibration of micro-optodes) has been suggested [104]:

$$I = I_0\left(\alpha + (1-\alpha)\frac{1}{1+k_{sv}c}\right) \tag{6}$$

In practical applications it has been shown that by applying an α value of around 0.15 this empirically derived equation describes the calibration curve of the $Ru(diph)_3$–based microoptode adequately [104]. The sensor signal is proportional to the O_2 partial pressure of the ambient water and proper sensor calibration requires only two calibration points, typically the readings obtained in anoxic and air-saturation conditions. Empirical relations based on polynomial regressions have also been applied for calibration of $Ru(diph)_3$–based mini- and microoptodes [101, 111]. Microoptodes have, as a result of the non-linear calibration curve, increased O_2 sensitivity in the range close to anoxia. Additionally, as a result of higher signal at low O_2 concentrations the signal to noise ratio improves, allowing for a better signal resolution. These advantages have been used for microoptode-based investigation of microaerophilic activity [111].

The signals of $Ru(diph)_3$–based optodes are not affected by changes in salinity [101, 104]. However, the fluorescence signal is dependent upon temperature, and ruthenium(II)-based complexes embedded in O_2-impermeable materials have actually been used for temperature sensing [114,115]. For PVC-immobilized fluorophores the I_0 value decreases almost linearly with temperature (0.5% °K^{-1}), while k_{SV} increases by approximately 1% °K^{-1} of temperature increase [116]. The net result is a decrease in O_2 sensitivity with increasing temperature which has to be accounted for during sensor calibration [101]. Preliminary data suggest that the temperature response is very sensor specific and that the temperature effect has to be quantified for each individual sensor [101,117]. In the case where optodes are used at constant temperatures the calibration should preferably be performed at the *in situ* temperature [100]. Temperature sensitivity is, however, very dependent on the immobilization material, and temperature-compensated microprobes applying combinations of fluorophore sensing chemistries can potentially be used for *in situ* work [108, 115].

3.3 CAPABILITIES AND LIMITATIONS

We still have very limited experience with *in situ* application of microoptodes and do not fully understand the details of their functioning under *in situ* conditions. However, their potential is promising and their main advantages seem to be a much simpler manufacturing procedure, no analyte consumption, and a superior stability to that of the Clark-type O_2 microelectrodes. Their main disadvantages are limited experience in their use, slower response times and a relatively high noise to signal ratio for the first prototypes. Still being a relatively new technique for the aquatic environment further instrumental optimization is probably required before the technique will be more generally applied.

3.3.1 Spatial and Temporal Resolution

In order to ensure sufficient fluorescence the minimal tip diameter of microoptodes is approximately 25 μm (alternatively very elaborate amplification instrumentation is required) [104]. The spatial resolution of microoptodes is consequently no better than around 50 μm (twice the outside tip diameter). Comparisons of microprofiles obtained with Clark-type O_2 microelectrodes (tip diameter < 10 μm) and microoptodes (tip diameter > 25 μm did not reveal any significant difference at a spatial resolution of 50 μm [104]. The larger tip size of microoptodes probably does not affect porewater measurements, but invasive measurements in, for example, aggregates, symbionts, or around individual microbiota may be problematic.

Microoptodes do not consume the analyte and consequently they have no stirring sensitivity. As discussed in section 2.3, this can be an advantage. The sensor signal is dependent upon a thermodynamic equilibrium, and the response time is significantly longer than for standard O_2 microelectrodes (Table 2). This is a consequence of the relatively thick sensing layers (which includes the optical isolation) and of the low O_2 permeability of mechanically stable immobilization materials. Microoptodes can be made with a faster response time by using materials with a higher permeability and a lower O_2 solubility (e.g. PVC) and by using thinner sensing layers. This, however, will be a trade-off with lower sensor stability and lower fluorescent signals (Table 2). In general, microoptodes are therefore not as suitable as microelectrodes for gross photosynthesis measurements or for studies on DBL O_2 dynamics.

3.3.2 Hydrostatic Pressure Effects

The relationship between hydrostatic pressure and the optode signal was investigated for Ru(diph)$_3$–polystyrene-based microoptodes [100]. The fluorescent

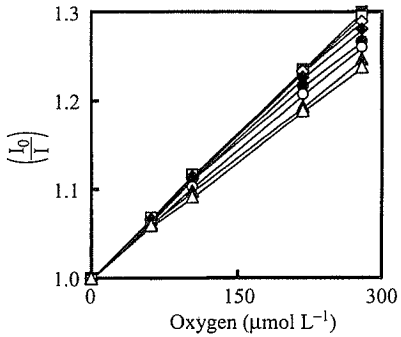

Figure 22. The effect of hydrostatic pressure on the Stern–Volmer plot of a Ru(Diph)$_3$ – PS – based microoptode. Measurements were performed at: 0.1 MPa (1 atm) (■–■); (5 MPa (50 atm) (□–□); 10 MPa (100 atm). (◇–◇); 20 MPa (200 atm.); (◆–◆); 30 MPa (300 atm) (●–●); 40 MPa (400 atm). (○–○); 50 MPa (500 atm) (▲–▲);60 MPa (600 atm). (△–△). A gradual decrease in O_2 sensitivity is apparent. Reprinted from *Deep-sea Res.*, **46**, 171 (1999) Glud *et al.*, with permission from Elsevier Science

signal in the absence of O_2 (I_0) showed a slight linear increase in the range of 0.1 – 60 MPa. The effect was ascribed to mechanical stress on the light guidance from the fluorophore to the measuring equipment. However, as the O_2 concentration of the ambient water was increased the effect of hydrostatic pressure became more pronounced and reached a maximum of 0.02 % atm^{-1} at surface air-saturation (301 μmol L^{-1}). The decreased quenching at elevated pressures caused a 20 % reduction in the O_2 sensitivity at a hydrostatic pressure equivalent to full ocean depth (60 MPa) (Figure 22). The sensors remained fully operational, and for *in situ* work at constant hydrostatic pressure, the effect is of minor importance, if calibration is performed *in situ* [100].

The decreased sensitivity is most likely related to a decrease in the O_2 permeability of the PS, but effects on the quenching process itself cannot be excluded. Microoptodes based on other immobilization materials (PVC and sol–gels) also express reduced sensitivity with increasing pressures [118]. Future applications of optodes for water column studies require a quantitative understanding of how the hydrostatic pressure affects the fluorescence signal.

3.3.3 *In Situ* Tests on a Benthic Lander

The first *in situ* measurements with microoptodes were recently performed [100] on a profiling lander and on a benthic chamber lander. Measurements were performed in a coastal sediment. The porewater profiles of the microoptodes were very similar to the profiles simultaneously obtained by Clark-type O_2 microelectrodes (Figure 23A). The optode measurements performed by the benthic chamber, however, appeared to be more 'noisy' than the comparable

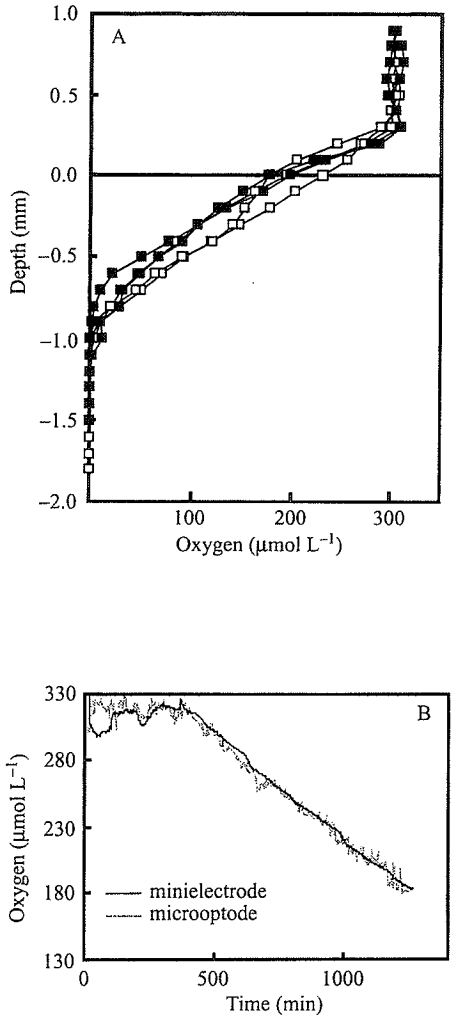

Figure 23. (A) *In situ* microprofiles measured simultaneously by Clark-type O_2 microelectrodes (open squares) and O_2 microoptodes (filled squares). Horizontal line indicates the estimated sediment surface. (B) Continuous recordings of a Clark-type O_2 mini-electrode and O_2 microoptode during an *in situ* incubation of a benthic chamber. The lid was closed approximately 450 min after deployment. Reprinted from *Deep-sea Res.*, **46**, 171, (1999) Glud *et al.*, , with permission from Elsevier Science

electrode measurements (Figure 23B). For the benthic chamber it was necessary to have a 1.5 m long optical fiber between the sensors and the measuring electronics [100]. The fluctuations in signal were most likely caused by bending of the fiber cable induced by water movements at the seafloor. This effect can be reduced by mechanical improvements, and be eliminated by lifetime-based measurements (see below).

3.3.4 Stability and Interference

Laboratory investigations have shown that after an initial phase (1–2 d) in which the sensitivity decreased (probably related to evaporation of solvents and material curing) the calibration characteristics of microoptodes remained constant for > 1 year. No significant drift was observed during continuous measurements with $Ru(diph)_3$–based optodes for periods up to 50 h [104]. Any signal drift is likely to be associated with photodegradation of the fluorophore. This can be reduced by exciting the fluorophore only at the frequency required for the measurements [100]. The excellent long-term stability of microoptodes can be further improved by using the fluorescence lifetime rather than the fluorescence intensity as a signal carrier [119]. The O_2 quenching is extremely specific for $Ru(diph)_3$–PS-based microoptodes, and interference by solutes of relevance for benthic *in situ* studies, i.e. pH, CO_2, H_2S, and heavy metals, has not been detected [104].

3.4 INTENSITY VERSUS LIFETIME-BASED MEASUREMENTS

The collisional quenching of molecular O_2 has two effects on the excited immobilized fluorophore: the fluorescent intensity is decreased and the lifetime of the fluorescence is shortened [120]. So far only the intensity-based measuring scheme has been developed for *in situ* O_2 measurements. The main problems associated with intensity-based measurements are the demand for a constant fluorescent signal, whereas microbending of the fibers will lead to noisy signals (see Figure 23B), and photodegradation and dye leaching will result in a loss of O_2 sensitivity. Further, in order to block out scattering and reflection effects, optical isolation of the sensor tip is required, even without any phototrophs in the surroundings.

The fluorescence lifetime signal is independent of the absolute light intensity, and thus avoids all of the potential problems related to intensity-based measurements. Lifetime-based O_2 microsensing has been realized in the laboratory [121] and for macrosensors used *in situ* [122]. The relationship between fluorescence lifetime and the partial pressure of O_2 is similar to equations (5) and (6) since:

$$\frac{\tau}{\tau_0} = \frac{I}{I_0} \tag{7}$$

where τ and τ_0 are the lifetimes of the fluorescence in the presence and absence of O_2, respectively [123]. For $Ru(diph)_3$-PS-based sensors τ_0 is around 4.5 μs while τ in 100 % O_2 is approximately 2 μs. These values are in a range still accessible by standard techniques for resolving lifetimes [121,123]. Other indicator molecules with longer lifetimes such as phosphorescent palladium and platinum porphyrins with lifetimes that are 20–100 times longer may, however, be considered for future lifetime-based *in situ* applications [108,124].

There are three principal techniques for determining luminescence lifetimes: (i) frequency domain method, (ii) ratioing method, (iii) and time domain method. Below we briefly present the various techniques but refer to the references mentioned below for a more thorough discussion of their various applications.

In the frequency domain method the fluorophore is excited with sinusoidally modulated light. The emitted light will reflect this modulation with a phase angle (φ), which is relatively easy to measure for a properly selected modulation frequency (f_{mod}). It is related to the fluorescence lifetime by: $\tan \varphi = \tau 2\pi f_{mod}$. This approach has been successfully applied in the laboratory for $Ru(diph)_3$–PS-based microoptodes [121, 123] and for water column, *in situ* measurements by applying a macrooptode based on a modified ruthenium complex immobilized in a sol–gel [122].

The ratioing method is based on a rectangular modulation of the excitation light (on/off), and the subsequent rise and decay of luminescence intensity contain information about the luminescence lifetime and can be quantified through simple ratioing of the signals in light and darkness. The method has been combined with imaging for medical applications [125].

In the time-domain method the immobilized fluorophore is exposed to an excitation pulse. Subsequently, the fluorescence intensity is quantified in well-defined time windows after the eclipse of light, and the fluorescence lifetime can be calculated from the exponential decay in fluorescence intensity. This approach has very recently been applied in combination with planar sensing for resolving two-dimensional O_2 distribution at benthic interfaces [126] (see section 3.5).

Lifetime-based methods have a promising potential for *in situ* O_2 measurements. However, the necessary measuring electronics are still relatively sophisticated and expensive [123], and further optimization and miniaturization is required before lifetime-based microoptodes can be applied *in situ*.

3.5 TWO-DIMENSIONAL OPTICAL SENSING

Microsensors measure the O_2 concentration at a single point and depth profiles are obtained by stepwise movement of the sensors. The oxygen distribution in many benthic communities is characterized by significant variations in time and space [127, 128]. Applying microsensors in order to describe or to overcome such variability may be an overwhelming task, and in bioturbated sediments, rhizospheres, biofilms, microbial mats etc. it can be virtually impossible. This has led into the development of sensor arrays that can apply up to eight microoptodes simultaneously within an area of approximately 10 cm^2 [123]. However, the horizontal resolution of such approaches is rather coarse and the number of microsensors that can be operated simultaneously is very limited. To overcome these problems, techniques based on medical applications of planar sensors combined with imaging were recently introduced in aquatic biology [116].

Instead of fixing the $Ru(diph)_3$–PS and the necessary optical insulation on the tip of a fiber (Figure 20) a transparent support foil was coated with the active gel layer. The 200 μm thick foils were glued onto one of the glass plates making up the side of a flume aquarium. The flume was then filled with sediment or microbial mats in such a way that the foil was partly covered (Figure 24). The excitation light was supplied by a halogen lamp equipped with an appropriate excitation filter. A CCD camera equipped with a 50 mm macro-lens and an emission filter recorded the two-dimensional distribution of fluorescent light (Figure 24). The images are calibrated using equation (6), but owing to inhomogeneities in the sensor and the applied light field each of the 3.4×10^5 measuring points making up the images was individually calibrated (the CCD chip contained 1317 × 1035 pixels, but images were obtained with a binning factor of 2). In the configuration described the calibrated oxygen images covered 13 × 17 mm and the oxygen concentration is expressed on an 8 bit scale at a spatial resolution of 26 × 26 μm. The planar optodes can resolve the O_2 distribution better than any traditional microsensor approach and allow for more detailed studies of the benthic O_2 dynamics (Figure 25A). The spatial resolution and the area covered by an image can be regulated by attaching appropriate optical lenses to the CCD camera. Sensor characteristics are the same as for the equivalent microoptodes described above. To what extent the placement of planar optodes affects the O_2 distribution at the investigated interface still remains to be studied in greater detail [116, 129]. Since the first demonstration of the measuring approach the technique has been successfully applied in other biological systems [129, 130].

Recently an optimized camera system applying lifetime-based imaging has been successfully combined with planar oxygen sensors for benthic interface studies [126]. The approach has interesting potential and offers many advantages compared with the intensity-based approach. The optical isolation layer

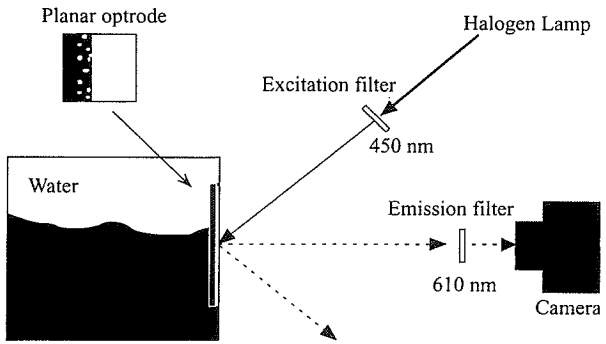

Figure 24. Basic set-up for the first planar optode measurements. An enlargement of the three-layered planar optode (support foil, sensing chemistry with Ti-granules and black silicone) is included. (Redrawn from Glud *et al.*, *Mar Ecol. Prog. Ser.*, **140**, 217 (1996))

can be omitted, which allows direct visual inspection of the sample during oxygen measurements [110].

So far the planar optode technique has been used only in the laboratory and requires further optimization before *in situ* applications can be realized. However, camera systems, based on the principle of inverted periscopes, have for some years been applied *in situ* for obtaining vertical images of biogenic structures in surficial sediments [131, 132]. Combining such camera systems with planar optodes should be possible in the coming years. This would represent a big step forward in studying the *in situ* oxygen dynamics at benthic interfaces.

4 CONCLUSIONS

A range of applicable O_2 microsensors is currently at our disposal for *in situ* investigations, and the lack of appropiate sensors is no longer a limiting factor for *in situ* investigations of O_2 dynamics. Clark-type O_2 microelectrodes probably represent the current 'state of the art'. However, microoptodes have potential advantages in areas of future *in situ* research. In general it is important to define the required sensor characteristics for a given task—and then to choose the proper sensor design. In some instances the optimal choice is to perform complementary measurements with different sensor types. Table 3 compiles the characteristics of O_2 micro- and mini-sensors discussed in this chapter with comments on prominent advantages and disadvantages.

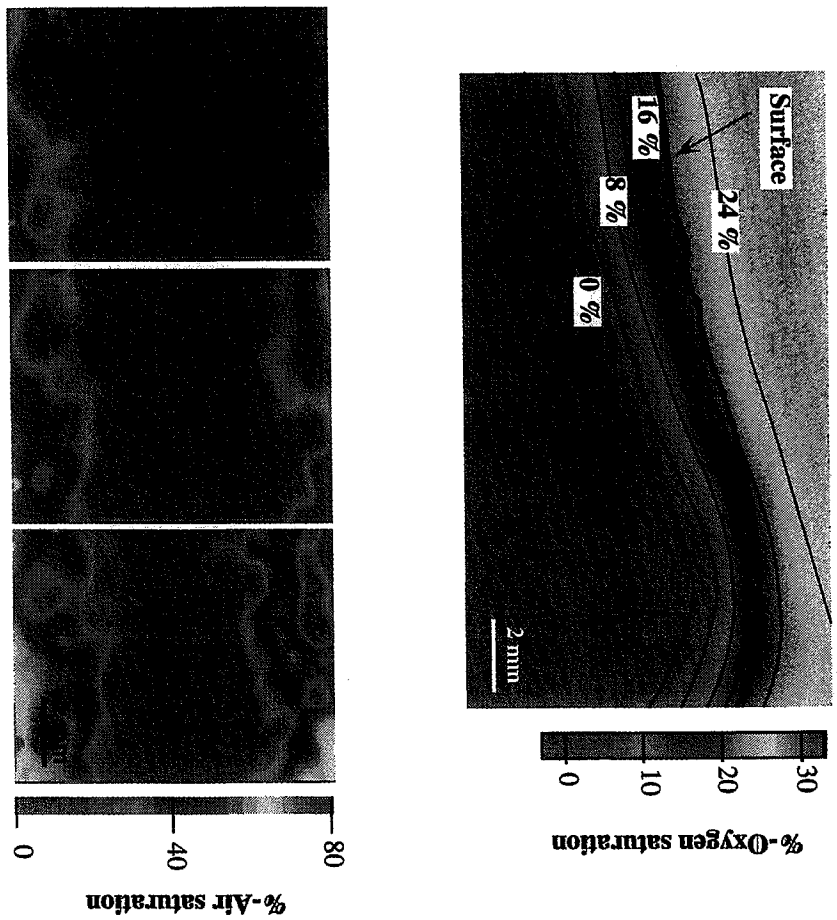

Plate 1 (Top) The O_2 distribution across the interface of an intertidal sediment as measured by an Ru(diph)$_3$–PS planar optode. Thin horizontal lines indicate the O_2 isopletes of 0, 4, 8, 12, 16, 20 and 24% air saturation. The thick line indicates the estimated position of the sediment surface. (Bottom) The O_2 distribution at the base of a 400μm thick biofilm, which was grown directly on the sensor at three different flow velocities: 20.5, 33.1 and 35.1cm s^{-1}. The better ventilation of the base film is apparent as the flow velocity is increased. (From Glud *et al.*, *Mar. Ecol. Prog. Ser.*, **140**, 217 (1996) and Glud *et al.*, *Aqua. Microb. Ecol.*, **14**, 223 (1998). Reproduced by permission of Inter-Research.

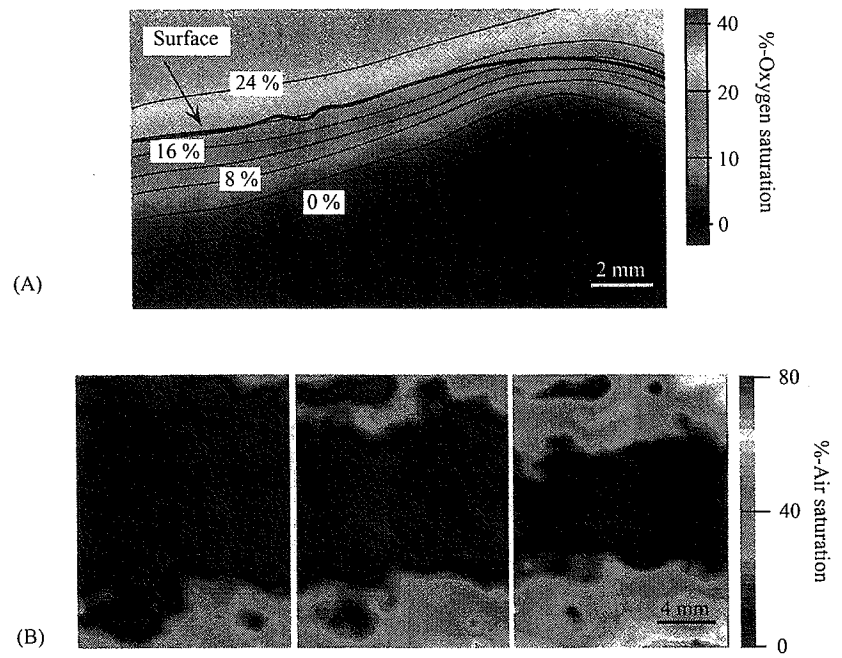

Figure 25. (A) The O_2 distribution across the interface of an intertidal sediment as measured by an Ru(diph)$_3$–PS planar optode. Thin horizontal lines indicate the O_2 isopletes of 0, 4,8,12,16,20 and 24 % air saturation. The thick line indicates the estimated position of the sediment surface. (B) The O_2 distribution at the base of a 400 μm thick biofilm, which was grown directly on the sensor at three different flow velocities: 20.5, 33.1 and 35.1 cm s^{-1}. The better ventilation of the base film is apparent as the flow velocity is increased. (From Glud *et al.*, *Mar. Ecol. Prog. Ser.*, **140**, 217 (1996) and Glud *et al.*, *Aqua. Microb. Ecol.*, **14**, 223 (1998). Reproduced by permission of Inter-Research.)

Table 3. Micro- and mini-sensors relevant for aquatic *in situ* investigations

Sensor type	Outside tip-diameter (μm)	Stirring sensitivity (%)	Response time t_{90} (s)	Long-term stability	Primary application areas	Prime references
DPX-coated cathode sensor	0.2–2	2–50	0.1–2	poor	Sediments/mats/biofilms Invasive approaches	16,32, 33
Needle DPX-coated cathode sensor	700	5–50	60–120	poor	Coarse or very oxic sediments	38
Clark-type microelectrode	1–10	0–2	0.5–2	good	Sediments/mats/biofilms Photosynthesis/water column/ respirometry / invasive approaches	40,45
Clark-type minielectrode*	1000–3000	2–5	0.2	good	Water column/ respirometry	22
$Ru(diph)_3$–PS microoptode	25–50	none	2–5	good†	Sediments/mats/biofilms/ water column/ respirometry	104,108
$Ru(diph)_3$–PS mini-needle optode‡	1000	none	250	good†	Coarse or very oxic sediments	94
$Ru(diph)_3$–PS planar optode	–	none	2–5	good†	Sediments/mats/biofilms Photosynthesis	116,126

* A comparable sensor for respirometry has been developed. That sensor has a longer response time but a superior stability[23].
† For optode measurements *in situ* lifetime-based sensing will further improve the sensor stability.
‡ A comparable sensor with a sol–gel matrix has been developed. That sensor has a tip diameter of 3 mm[101].

ACKNOWLEGDEMENTS

Following funding agencies are gratefully acknowledged for their financial support: The Danish National Science Research Council, the European Commission, and the Carlsberg Foundation. Rodney Roberts is thanked for his help with improving the language.

GLOSSARY

CCD camera Charged coupled device camera.
CTD Conductivity, temperature, and depth instrument.
DPX resin resin for microelectrode (Fig 1) = n-(2-methyl-4-amino-5-pyrimidyl)-n-(1-methyl-2-thiopbut(1)en-4-diphosphatidyl) amide
Benthic In relation to the sea bottom.
Diffusion layer (DL) The region around a sensor tip where diffusion is the main transport mode.
Diffusive boundary layer (DBL) The horizon above a substratum where diffusion is the main transport mode.
Interface Boundary between sediment (or any other substratum) and water phase.
Lander Independent vehicle operating at the sea floor.
Pelagic In relation to the water column far from sea shore.
Sol–gel (ormosil) Condensed silica alkoxides.
Stirring sensitivity Change in sensor signal caused by change in ambient water flow

LIST OF SYMBOLS

(the point of first use is given in parentheses)

c	Concentration
c_w	Concentration in water, infinitely far away from the sensor
c_2	Concentration at the sensor surface
D	Diffusion coefficient
D_e	Diffusion coefficient in electrolyte
f	Fugacity
f_0	Fugacity at water surface
f_{mod}	Modulation frequency
I	Fluorescence intensity
I_0	Fluorescence intensity in absence of O_2
J	Diffusive flux
k_{SV}	Quenching coefficient

p_w	Partial pressure in ambient water
ΔP	Hydrostatic pressure
R	Gas constant
r	Radius
S_e	Solubility in electrolyte
Si	Electrode signal
ST	Stirring sensitivity
T	Absolute temperature
t_{90}	90% response time
v	partial molar volume
Z_m	Membrane length
Z_e	Distance within the electrolyte
Ψ	Permeability
Φ	Current generated by O_2 reduction
φ	Phase angle
τ	Fluorescence lifetime
τ_0	Fluorescence lifetime in absence of O_2

REFERENCES

1. Winkler, L. W. (1888). Die Bestimmung des im Wasser gelösten Sauerstoffes, *Ber. Dtsch. Chem. Ges. Berlin*, **21**, 2843.
2. Scholander, P. F., van Dam, L., Claff, C. L. and Kanwisher, J. W. (1955). Microgasometric determination of dissolved oxygen and nitrogen *Biol. Bull.*, **109**, 328.
3. Benson, B. B. and Parker, P. D. M. (1961). Relations among the solubilities of nitrogen, argon and oxygen in distilled water and sea water, *J. Phys. Chem.*, **65**, 1489.
4. Swinnerton, J. W., Linnebom V. J. and Cheek C. H. (1962). Determination of dissolved gases in aqueous solutions by gas chromatography *Anal. Chem.*, **34**, 483.
5. Davies, P. W. and Brink, F. (1942). Microelectrodes for measuring local oxygen tension in animal tissue, *Rev. Sci. Instrum.* **13**, 524.
6. Sproule, B. J., Miller, W. F., Cushing, I.E. and Chapman, C. B. (1957). An improved polarographic method of measuring oxygen tension in whole blood, *J. Appl. Physiol.*, **30**, 272.
7. Kanwisher, J. (1959). A polarographic oxygen electrode, *Limnol. Oceanogr.*, **4**, 210.
8. Davison, W. and Whitfield, M. (1977). Modulated polarographic and voltametric techniques in the study of natural water chemistry, *J. Electroanal. Chem.*, **75**, 763.
9. Yim, H. S. and Meyerhoff, M. E. (1992). Reversible potentiometric oxygen sensors based on polymeric and metallic film electrodes, *Anal. Chem.*, **64**, 1777.
10. Brendel P. J. and Luther, III G. W. (1995). Development of a gold amalgam voltametric microelectrode for the determination of dissolved Fe, Mn, O_2, and S^{2-} of marine and freshwater sediments, *Environ. Sci. Technol.*, **29**, 751.
11. Atkinson, M. J., Thomas, F. I. M., Terrill, E., Morita, K. and Liu, C. C. (1995). A micro-hole potentiostactic oxygen sensor for oceanic CTD's, *Deep-sea Res.*, **42**, 761.

12. Fatt, I. (1976). *Polarographic Oxygen Sensor*, CRC Press, Cleveland, OH, 279 pp.
13. Gnaiger E. and Forstner, H. (1983). *Polarographic Oxygen Sensors*, Springer, Berlin, 370 pp.
14. Smith, K. L., Jr. and Baldwin, R. J. (1983). Deep-sea respirometry: In situ techniques. In *Polarographic Oxygen Sensors*, ed. Gnaiger, E. and Forstner, H., Springer, p. 37.
15. Thomas, F. I. M., McCarthy, S. A., Bower, J., Krothapalli, S., Atkinson, M. J. and Flament, P. (1995). Response characteristics of two oxygen sensors for oceanic CTD's, *J. Atmos. Ocean. Technol* **12**, 687.
16. Revsbech, N. P. and Jorgensen, B. B. (1986). Microelectrodes: their use in microbial ecology, *Adv. Microb. Ecol.*, **9**, 293.
17. Warren, B. A. (1973). The transpacific hydrographic sections at Lats. 43 °S and 28 °S: the SCORPIO Expedition—II. Deep water. *Deep-Sea Res.*, **20**, 9.
18. Archer, D. and Devol., A. (1992). Benthic oxygen fluxes on the Washington shelf and slope: A comparison of in situ microelectrode and chamber measurements. *Limnol. Oceanogr.*, **37**, 614.
19. Revsbech, N. P., Jørgensen, B. B. and Blackburn, T. H., (1980). Oxygen in the seabottom measured with a microelectrode, *Science*, **207**, 1355.
20. Revsbech, N. P., Sorensen, J., Blackburn, T. H. and Lomholt, J. P. (1980). Distribution of oxygen in marine sediments measured with microelectrodes, *Limnol. Oceanogr.*, **25**, 403.
21. Chen, Y.S. and Bungay, H. R. (1981). Microelectrode studies of oxygen transfer in trickling filter slimes, *Biotech. Bioeng.*, **23**, 781.
22. Oldham, C. (1994). A fast-response oxygen sensor for use on fine scale and microstructure CTD-profiles, *Limnol Oceanogr.*, **39**, 1959.
23. Glud, R. N., Gundersen, J. K., Revsbech, N. P., Jorgensen, B. B. and Hüttel, M. (1995). Calibration and performance of the stirred flux chamber from the benthic lander Elinor, *Deep-sea Res.*, **42**, 1029.
24. Kuenen, J. G., Jørgensen B. B. and Revsbech N. P. (1986). Oxygen measurements in trickling filter biofilms, *Wat. Res.*, **20**, 1589.
25. Sweerts J. P. R. A, Louis V. and Cappenberg T. E. (1989). Oxygen concentration profiles and exchange in sediment cores with circulating overlying water, *Fresh. Biol.*, **21**, 401.
26. Jorgensen, B. B. and Des Marais, D. J. (1990). The diffusive boundary layer of sediments: Oxygen microgradients over a microbial mat, *Limnol. Oceanogr.*, **35**, 1343.
27. Kühl, M., Cohen, Y., Dalsgaard, T., Jørgensen, B. B. and Revsbech N. P. (1995). Microenvironment and photosynthesis of zooxanthellae in scleratinian corals studied with microsensors for O_2, pH, and light, *Mar. Ecol. Prog. Ser.*, **117**, 159.
28. Ploug, H., Kühl, M., Buchholz, B. and Jørgensen, B. B. (1997). Anoxic aggregates–an emphemeral phenomenon in the ocean, *Aquat. Microb. Ecol.*, **13**, 285.
29. Whalen, W. J., Riley J. and Nair P. (1967). A microelectrode for measuring intracellular pO_2, *J. Appl. Physiol.*, **23**, 798.
30. Bungay H. R. (1969). Microprobe technique for determining diffusivities and respiration rates in microbial slime systems, *Biotech. Bioeng.*, **11**, 765.
31. Baumgärtl H. and Lübbers D. W. (1973). Platinum needle electrodes for polarographic measurement of oxygen and hydrogen. In *Oxygen Supply*, ed. Kessler, M. Urban and Schwarzenberg, München, p. 130.
32. Baumgärtl, H. and Lübbers D. W. (1983). Microcoaxial needle sensor for polarographic measurements of local O_2 pressure in the cellular range of living tissue. Its

construction and properties. In *Polarographic Oxygen Sensors*, (ed. Gnaiger, E. and Forstner, H., Springer, Berlin, p. 37.
33. Revsbech, N. P. (1983). *In situ* measurements of oxygen profiles of sediments by use of oxygen microelectrodes. In *Polarographic Oxygen Sensors*, (ed. Gnaiger, E. and Forstner, H., Springer, Berlin, p. 265.
34. Gust G., Booij K., Helder W. and Sundby B., (1987). On the velocity sensitivity (stirring effect) of polarographic oxygen microelectrodes, *Neth. J. Sea Res.*, **21**, 255.
35. Epping, E., and Helder , W. (1997). Oxygen budgets for Northern Adriatic sediments calculated from in situ oxygen microprofiles, *Contin. Shelf Res.*, **17**, 1737.
36. Revsbech, N. P., Sørensen, J., Blackburn, T. H. and Lomholt, J. P. (1980). Distribution of oxygen in marine sediments measured with microelectrodes, *Limnol. Oceanogr.*, **25**, 403.
37. Reimers, C. E., Kalhorn S., Emerson, S. R and Nealson, K. H. (1984). Oxygen consumptiom rates in pelagic sediments from the Central Pacific: First estimates from microelectrode profiles, *Geochim. Cosmochim. Acta.*, **48**, 903.
38. Helder, W. and Bakker, J.F. (1985). Shipboard comparison of micro and minielectrodes for measuring oxygen distribution in marine sediments, *Limnol. Oceanogr.*, **30**, 1106.
39. Visscher, P. T., Beukema, J. and van Germerden, H. (1991). In situ measurements of oxygen and sulfide profiles with a novel combined needle-electrode, *Limnol. Oceanogr.*, **36**, 1476.
40. Revsbech, N. P. and Ward, D. (1983). Oxygen microelectrode that is insensitive to medium chemical composition: Use in an acid microbial mat dominated by *Cyanidium caldarium*, *Appl. Environ. Microbiol.*, **45**, 755.
41. Clark, L. C., Wolf, R., Granger, D. and Taylor A. (1953). Continuous recording of blood oxygen tension by polarography, *J. Appl. Physiol.*, **6**, 183.
42. Tengberg A., De Bovee, F., Hall, P., Berelson, W., Cicceri, G., Crassous, P., Devol, A., Emerson, S., Glud, R. N., Graziottin, F., Gundersen, J. K., Hammond, D., Helder, W., Holby, O., Jahnke, R., Khripounoff, A., Nuppenau, V., Pfannkuche, O., Reimers, C., Rowe, G., Sahami, A., Sayles, F., Schuster, M., Wehrli, B. and De Wilde, P. (1995). Benthic chamber and profile landers in oceanography—A review of design, technical solutions and functioning, *Prog. Oceanogr.*, **35**, 253.
43. Reimers, C. E., Jahnke, R. A. and Thomsen, L. (1999). In situ boundary layer measurements. In *The Benthic Boundary Layer: Transport and Biogeochemical Processes*, (ed. Boudreau, B. and Jorgensen, B. B., Oxford University Press, Oxford.
44. Reimers, C. E. and Glud, R. N. (2000). In situ chemical measurements at the sediment–water interface. In *Chemical Sensors in Oceanography*, (ed. Varney, M., Gordon and Breach.
45. Revsbech, N. P., (1989). An oxygen microelectrode with a guard cathode, *Limnol. Oceanogr.*, **34**, 474.
46. Bucher, R., (1983). Electrolytes. In *Polarographic Oxygen Sensors*, (ed. Gnaiger, E. and Forstner, H., Springer, Berlin, p. 66.
47. Gundersen, J. K., Jorgensen, B. B., Larsen, E. and Jannasch, H. W. (1992). Mats of giant sulphur bacteria on deep-sea sediments due to fluctuating hydrothermal flow, *Nature*, **360**, 454.
48. Berntsson, M. A., Tengberg, A., Hall, P. O. J. and Josefson, M. (1998). Multivariate experimental methodology applied to the calibration of a Clark-type oxygen sensor, *Anal. Chim. Acta.*, **355**, 43.

49. Gundersen, J. K., Ramsing, N. B. and Glud, R. N. (1998). Predicting the signal of O_2 microsensors from physical dimensions, salinity and O_2 concentration, *Limnol. Oceanogr.*, **43**, 1932.
50. Crank, J. (1989). *The Mathematics of Diffusion*, Clarendon Press, Oxford, 414 pp.
51. Garcia, H. E. and Gordon, L. I. (1992). Oxygen solubility in seawater: Better fitting equations, *Limnol. Oceanogr.* **37**, 1307.
52. Broecker, W. S. and Peng, T. H. (1974). Gas exchange rates between air and sea, *Tellus.*, **26**, 21.
53. Li, Y. H. and Gregory, S. (1974). Diffusion of ions in deep-sea sediments, *Geochim. Cosmochim. Acta*, **38**, 703.
54. Millard, R. C. (1982). CTD calibration and data processing techniques at WHOI using 1978 practical salinity scale. In *Proc. Intl STD Conf. Workshop*, Mar. Rech. Soc., 19 pp.
55. Mancy, K. H., Okun, D. A. and Reilley, C. N. (1962). A galvanic cell oxygen analyzer, *J. Electroanal. Chem.*, **4**, 65.
56. Revsbech, N. P., personal communication.
57. Wenzhöfer, F., Holby, O., Glud R. N., Nielsen, H. K. and Gundersen, J. K. (2000). In situ microsensor studies of a hydrothermal vent at Milso (Greece), *Mar. Chem.*, **69**, 43.
58. Quetin, L. B. and Mickel, T. J. (1983). Sealed respirometers for small invertebrates. In *Polarographic Oxygen Sensors* (ed. Gnaiger, E. and Forstner, H., Springer, Berlin, p. 184.
59. Hale, J. M. (1983). Factors influencing the stability of polarographic oxygen sensors. In *Polarographic Oxygen Sensors*, (ed. Gnaiger, E. and Forstner, H., Springer, Berlin, p. 3.
60. Revsbech, N. P., Nielsen, L. P. and Ramsing, N. B. (1998). A novel microsensor principle for determination of apparent diffusivity in sediments, *Limnol. Oceanogr.*, **43**, 986.
61. Jirka, G. H. and Ho, A. H. W. (1990). Measurements of gas concentration fluctuations at the water surface, *J. Hydraul. Eng.*, **116**, 835.
62. Bühler, H. (1983). A double-membrane sterilizable oxygen sensor. In *Polarographic Oxygen Sensors*, (ed. Gnaiger, E. and Forstner, H., Springer, Berlin p. 76.
63. Gnaiger, E. (1983). In situ measurement of oxygen profiles in lakes: Microstratifications, oscillations and the limits of comparison with chemical methods. In *Polarographic Oxygen Sensors* ed. Gnaiger, E. and Forstner, H., Springer, Berlin, p. 245.
64. Glud, R. N., Gundersen, J. K., Revsbech, N. P., Jorgensen, B. B. and Hüttel, M. (1995). Calibration and performance of the stirred flux chamber from the benthic lander Elinor, *Deep-sea Res.*, **42**, 1029.
65. Rink, S., Kühl, M., Bijma, J. and Spero, H. J. (1998). Microsensor studies of photosynthesis and respiration in the symbiotic foraminifer, *Orbulina universa*, *Mar. Biol.*, **131**, 583.
66. Plough, H. and Jorgensen, B. B. (1999). A net-jet flow system for mass transfer and microsensor studies of sinking aggregates, *Mar. Ecol. Prog. Ser.*, **176**, 279.
67. Albanese, R. A. (1973). On microelectrode distortion of tissue oxygen tensions, *J. Theor. Biol.*, **38**, 143.
68. Boudreau, B. P. and Guinasso, N. L. (1982). The influence of a diffusive sublayer on accretion, dissolution, and diagenesis at the sea floor. In *The Dynamic Environment of the Ocean Floor*, ed. Fanning, K. A. and Manheim, F. T., Lexington, pp. 115–145.
69. Jorgensen, B. B. and Revsbech, N. P. (1985). Diffusive boundary layers and the oxygen uptake of sediments and detritus, *Limnol. Oceanogr.*, **30**, 111.

70. Archer, D., Emerson, S. and Smith, C. R. (1989). Direct measurement of the diffusive sublayer at the deep sea floor using oxygen microelectrodes, *Nature* **340**, 623.
71. Gundersen J. K. and Jorgensen, B. B. (1990). Microstructure of diffusive boundary layers and the oxygen uptake of the sea floor, *Nature* **345**, 604.
72. Glud, R. N, Gundersen, J .K., Jorgensen, B. B., Revsbech, N. P. and Schulz, H. D. (1994). Diffusive and total oxygen uptake of deep-sea sediments in the eastern South Atlantic Ocean: *In Situ* and laboratory measurements, *Deep Sea Res.*, **41**, 1767.
73. Jorgensen, B. B. (1994). Diffusion processes and boundary layers in microbial mats. In *Microbial Mats*, (ed. Stal, L. J. and Caumette, P., NATO ASI Series, Vol. G35.
74. Rasmussen, H. and Jorgensen, B.B. (1992). Microelectrode studies of seasonal oxygen uptake in a coastal sediment: role of molecular diffusion, *Mar Ecol. Prog. Ser.*, **81**, 289.
75. Ullman, W. J. and Aller R. C. (1982). Diffusion coefficients in nearshore marine sediments, *Limnol. Oceanogr.*, **27**, 552.
76. Iversen, N. and Jorgensen, B.B. (1993). Diffusion coefficients of sulfate and methane in marine sediments: Influence of porosity, *Geochim Cosmochim Acta.*, **75**, 571.
77. Klimant, I., Holst, G. and Kühl, M. (1997). A simple fiber-optic sensor to detect the penetration of microsensors into sediments and other biological materials, *Limnol. Oceanogr.*, **42**, 1638.
78. Reimers, C. E. (1992). Carbon fluxes and burial rates over the continental slope and rise off central California with implications for the global carbon cycle, *Glob. Biogeochem.* **6**, 199.
79. Sweertz J. P. R. A., Lois, V. and Cappenberg, T. E. (1989). Oxygen concentration profiles and exchange in sediment cores with circulating overlying water, *Fresh. Biol.*, **21**, 401.
80. Glud, R. N., Gundersen, J. K., Revsbech, N. P. and Jorgensen B. B. (1994). Effects on the benthic diffusive boundary layer imposed by microelectrodes, *Limnol. Oceanogr.*, **39**, 462.
81. Lorenzen, J., Glud, R. N. and Revsbech, N. P. (1995). Impact of microsensor caused changes in diffusive boundary layer thickness on O_2 profiles and photosynthetic rates in benthic communities of microorganisms, *Mar. Ecol. Prog. Ser.*, **119**, 237.
82. Epping E. H. G. and Jorgensen, B. B. (1995). Light enhanced oxygen respiration in benthic phototrophic communities, *Mar. Ecol. Prog. Ser.*, **139**, 193.
83. Kühl, M., Glud, R. N., Ploug, H. and Ramsing N. B. (1996). Microenvironmental control of photosynthesis and photosynthesis-coupled respiration in an epilithic cyanobacterial biofilm, *J. Phycol.*, **32**, 799.
84. Revsbech N. P. and Jorgensen, B. B. (1983). Photosynthesis of benthic microflora measured with high spatial resolution by the microprofile method: capabilities and limitations of the method, *Limnol. Oceanogr.*, **28**, 749.
85. Glud, R. N., Ramsing, N. B. and Revsbech, N. P. (1992). Photosynthesis and photosynthesis-coupled respiration in natural bio-films quantified with microsensors, *J. Phycol.*, **28**, 51.
86. Lassen, C., Glud, R. N., Ramsing, N. B. and Revsbech N. P. (1998). A method to improve the spatial resolution of photosynthetic rates obtained by oxygen microsensors, *J. Phycol.* **34**, 89.
87. Jost, W. (1964). Fundamental aspects of diffusion processes, *Angew. Chem. Int. Ed. Engl.*, **3**, 713.

88. Enns T., Scholander, P. F. and Bradstreet, E. D. (1965). Effect of hydrostatic pressure on gases dissolved in water, *J. Phys. Chem.*, **69**, 389.
89. Reimers, C. E. (1987). An in situ microprofiling instrument for measuring interfacial pore water gradients: methods and oxygen profiles from North Pacific Ocean, *Deep-sea Res.*, **34**, 2019.
90. Greene, M. W., Gafford, R. D. and Rohrbaugh, D. G. (1970). A continuous profiling deep-submersible, dissolved monitor, *Mar. Technol. Soc.*, **2**, 1485.
91. Morild, E. and Olmheim, J. E. (1980). Pressure dependence of the oxygen electrode, *J. Electrochem. Soc.*, **127**, 2356.
92. Owens, W. B. and Millard, R. C., Jr. (1985). A new algorithm for CETD oxygen calibration, *J. Phys. Oceanogr.*, **15**, 621.
93. Atkinson, M. J., Thomas, F. I. M. and Larson, N. (1996). Effect of pressure on oxygen sensors. *J. Atm. Oceanic Technol..*, **13**, 1267.
94. Wenzhöfer, F., Holby, O. and Kohls, O. (1999). Deep penetrating oxygen profiles measured in situ by oxygen optodes, *Deep-sea Res.*, in press.
95. Glud, R. N., Gundersen, J. K. and Holby, O. (1999). Benthic in situ respiration in the upwelling area off central Chile, *Mar. Ecol. Prog. Ser.*, **186**, 9.
96. Kühl, M. and Revsbech, N. P. (2000). Microsensors for the study of interfacial biogeochemical processes. In *The Benthic Boundary Layer: Transport and Biogeochemical Processes*, (ed. Boudreau, B. and Jorgensen, B. B., Oxford University Press, Oxford.
97. Kroneis, H. W. and Marsoner, H. J. (1983). A fluorescence-based sterilizable oxygen probe for use in bioreactors, *Sens. Actuators*, **4**, 587.
98. Peterson, J. I., Fitzgerald, R. V. and Buckhold, D. K. (1984). Fiber-optic probe for in vivo measurement of oxygen partial pressure, *Anal. Chem.*, **56**, 474.
99. Leiner, M. J. P. (1991). Luminescence chemical sensors for biomedical applications: Scope and limitations, *Anal. Chim. Acta*, **225**, 209.
100. Glud, R. N., Klimant, I., Holst, G., Kohls, O., Meyer, V., Kühl, M. and Gundersen, J. K. (1999). Adaptation, test and *in situ* measurements with O_2 microoptodes on benthic landers, *Deep-sea Res.*, **46**, 171.
101. Wang, W., Reimers, C. E., Shahriari, M. and Wainright, S. C. (1999). A fiber optic sensor for monitoring the variability of dissolved oxygen in the coastal zone. In Proceedings of The Marine Technology Society, Annual Conference, 1998.
102. Kohls, O. (1995). Optische Sauerstoffsensoren. Ph.D. thesis, University Hannover.
103. Kautsky, H. (1939). Quenching of luminescence by oxygen, *Trans. Faraday Soc.*, **35**, 216.
104. Klimant, I., Meyer, V. and Kühl, M. (1995). Fiber-optic oxygen microsensors, a new tool in aquatic biology, *Limnol. Oceanogr.*, **40**, 1159.
105. Wolfbeis, O. S., Leiner, M. J. P. and Posch, H. E. (1986). A new sensing material for optical oxygen measurement with the indicator embedded in an aqueous phase, *Microchim. Act*, **3**, 359.
106. Bacon, J. R. and Demas, J. N. (1987). Determination of oxygen concentration by luminescence quenching of a polymer immobilized transition-metal complex, *Anal. Chem.*, **59**, 2780.
107. Klimant, I. and Wolbeis, O. S. (1995). Oxygen sensitive luminescent materials based on silicone-soluble ruthenium diimine complexes, *Anal. Chem.*, **34**, 3160.
108. Klimant, I., Kühl, M., Glud, R. N. and Holst, G. (1997). Optical measurement of oxygen and temperature in microscale: strategies and biological applications, *Sens. Actuators*, **38–39**, 29.

109. McEvoy, A. K., McDonagh, C. M. and MacCraith, B. D. (1996). Dissolved oxygen sensor based on fluorescence quenching of oxygen sensitive ruthenium complexes immobilised in Sol–Gel derived porous silica coatings, *Anal.*, **121**, 785.
110. Koenig, B., Holst, G., Glud, R. N. and Kühl, M. (2000). Imaging of oxygen distribution at benthic interfaces: A mini-review . In *Organism–Sediment Interactions*, (ed. J. Y. Aller, Woodin, S. A., and Aller, R. C.). The Belle W. Baruch Library in Marine Science, in press.
111. Riess, W., Giere, O., Kohls, O. and Sarbu, S. M. (1999). Anoxic thermomineral waters and bacterial mats a habitat for freshwater nematodes, *Aquat. Microb. Biol.*, **18**, 157.
112. Stern, O., and Volmer, M., (1919). Über die Abklingzeit der Fluoreszenz, Phys. Z. **20**, 183.
113. Carraway, E. R., Demas, J. N. and DeGraff, B. A. (1991). Luminescence quenching mechanisms for microheterogenous systems, *Anal. Chem.*, **63**, 332.
114. Demas, J. N. and DeGraff, B. A. (1992). On the design of luminescence based temperature sensors, *Proc. SPIE*, **1796**, 71.
115. Holst, G., Kühl, M. and Klimant, I. (1996). New temperature micro-optodes. In *Abstracts 3rd Eur. Conf. Optical Chemical Sensors and Biosensors (EUROPT(R)ODE III)*, Zurich, Switzerland.
116. Glud, R. N., Ramsing, N. B., Gundersen, J. K. and Klimant, I. (1996). Planar optrodes, a new tool for fine scale measurements of two dimensional O_2 distribution in benthic communities, *Mar. Ecol. Prog. Ser.*, **140**, 217.
117. Klimant, I, personal communication.
118. Kohls, O. and colleagues, unpublished results.
119. Lippitsch, M. E., Pusterhoffer, J., Leiner, M. J. P. and Wolfbeis, O. (1988). Fiber-optic oxygen sensor with the fluorescence decay time as the information carrier, *Anal. Chim. Acta.*, **205**, 16.
120. Lübbers D. W. (1992). Fluorescence based chemical sensors, *Adv. Biosensors*, **2**, 215.
121. Holst, G., Kühl, M. and Klimant, I. (1995). A novel measuring system for oxygen microoptodes based on a phase modulation technique, *SPIE Proc.*, **2508**, 387.
122. Kohls, O. and colleagues (1999). Work in progress.
123. Holst, G., Glud, R. N., Kühl, M. and Klimant, I. (1997). A microoptode array for fine-scale measurement of oxygen distribution, *Sens. Actuators*, **38–39**, 122.
124. Papkovsky, D. B. (1995). New oxygen sensors and their application to biosensing, *Sens. Actuators*, **29**, 213.
125. Hartman, P., Ziegler, W., Holst, G. and Lübbers, D. W. (1997). Oxygen flux fluorescence lifetime imaging, *Sens. Actuators* **38–39**, 110.
126. Holst, G., Kohls, O., Klimant, I., König, B., Kühl, M. and Richter, T. (1998). A modular luminescence lifetime imaging system for mapping oxygen distribution in biological samples, *Sens. Actuators*, **51**, 163.
127. Jorgensen, B. B., Revsbech, N. P. and Cohen, Y. (1983). Photosynthesis and structure of benthic microbial mats: Microelectrode and SEM studies of four cyanobacterial communities, *Limnol. Oceanogr.*, **28**, 1075.
128. Glud, R. N., Holby,O., Hofmann, F. and Canfield, D. (1998). Benthic mineralization in Arctic sediments (Svalbard), *Mar. Ecol. Prog. Ser.*, **173**, 237.
129. Glud, R. N., Santegoeds, C. M., de Beer, D., Kohls, O. and Ramsing, N. B. (1998). Oxygen dynamics at the base of a biofilm studied with planar optrodes, *Aquat. Microb. Ecol.*, **14**, 223.

130. Glud, R. N., Kühl, M., Kohls, O. and Ramsing N. B. (1999). Heterogeneity of oxygen production and consumption in a photosynthetic microbial mat as studied by planar optodes, *J. Phycol.*, **35**, 270.
131. Rhoads, D. C. and Germano, J. D. (1982). Characterization of organism–sediment relations using sediment profile imaging: An efficient method of remote ecological monitoring of the seafloor (Remots system), *Mar. Ecol. Prog. Ser.*, **8**, 115.
132. Grehan, A. J. Keegan, B. F., Bhaud, M. and Guille, A. (1992). Sediment profile imaging of soft substrates in the western Mediterranean: The extent and importance of faunal reworking, *C. R. Acad. Sci. Paris*, **309**, 315.